Biosensors and Bioelectronics 225 (2023) 115100

Contents lists available at ScienceDirect

Biosensors and Bioelectronics

journal homepage: www.elsevier.com/locate/bios

Biosensor integrated brain-on-a-chip platforms: Progress and prospects in clinical translation

Berivan Cecen [a,b], Ecem Saygili [c], Iman Zare [d], Omid Nejati [e], Danial Khorsandi [f], Atefeh Zarepour [g], Emine Alarcin [h], Ali Zarrabi [g], Seda Nur Topkaya [i], Ozlem Yesil-Celiktas [c,j,***], Ebrahim Mostafavi [k,l,**], Ayça Bal-Öztürk [e,m,*]

[a] Department of Mechanical Engineering, Rowan University, Glassboro, NJ, 08028, USA
[b] Department of Biomedical Engineering, Rowan University, Glassboro, NJ, 08028, USA
[c] Department of Bioengineering, Faculty of Engineering, Ege University, 35100, Izmir, Turkey
[d] Research and Development Department, Sina Medical Biochemistry Technologies Co. Ltd., Shiraz, 7178795844, Iran
[e] Department of Stem Cell and Tissue Engineering, Institute of Health Sciences, Istinye University, 34010, Istanbul, Turkey
[f] Terasaki Institute for Biomedical Innovation, Los Angeles, 90064, CA, USA
[g] Department of Biomedical Engineering, Faculty of Engineering and Natural Sciences, Istinye University, 34396, Istanbul, Turkey
[h] Department of Pharmaceutical Technology, Faculty of Pharmacy, Marmara University, Istanbul, Turkey
[i] Department of Analytical Chemistry, Faculty of Pharmacy, Izmir Katip Celebi University, Izmir, Turkey
[j] EgeSAM-Ege University Translational Pulmonary Research Center, Bornova, Izmir, Turkey
[k] Stanford Cardiovascular Institute, Stanford University School of Medicine, Stanford, CA, 94305, USA
[l] Department of Medicine, Stanford University School of Medicine, Stanford, CA, 94305, USA
[m] Department of Analytical Chemistry, Faculty of Pharmacy, Istinye University, 34010, Zeytinburnu, Istanbul, Turkey

ARTICLE INFO

Keywords:
Brain-on-a-chip
Biosensor
Integrated biosensors
Microphysiological systems
Microfluidics
Organ-on-Chip
Microfabrication

ABSTRACT

Because of the brain's complexity, developing effective treatments for neurological disorders is a formidable challenge. Research efforts to this end are advancing as *in vitro* systems have reached the point that they can imitate critical components of the brain's structure and function. Brain-on-a-chip (BoC) was first used for microfluidics-based systems with small synthetic tissues but has expanded recently to include *in vitro* simulation of the central nervous system (CNS). Defining the system's qualifying parameters may improve the BoC for the next generation of *in vitro* platforms. These parameters show how well a given platform solves the problems unique to *in vitro* CNS modeling (like recreating the brain's microenvironment and including essential parts like the blood-brain barrier (BBB)) and how much more value it offers than traditional cell culture systems. This review provides an overview of the practical concerns of creating and deploying BoC systems and elaborates on how these technologies might be used. Not only how advanced biosensing technologies could be integrated with BoC system but also how novel approaches will automate assays and improve point-of-care (PoC) diagnostics and accurate quantitative analyses are discussed. Key challenges providing opportunities for clinical translation of BoC in neurodegenerative disorders are also addressed.

1. Introduction

The brain is the most complex organ in the human body (Akhtar et al., 2021; Vieira de Sá et al., 2021). The skull protects the brain from mechanical stress, while the blood-brain barrier (BBB) protects the brain from external toxins (Liang and Yoon, 2021; Teleanu et al., 2022). To maintain the physical and chemical stability of the neuronal microenvironment, the BBB limits molecular transit between circulation and the brain parenchyma (Sullivan et al., 2022; Zhao et al., 2022). Types of cell configuration, tight junction proteins, selective permeability, and shear

* Corresponding author. Department of Stem Cell and Tissue Engineering, Institute of Health Sciences, Istinye University, 34010, Istanbul, Turkey.
** Corresponding author. Department of Medicine, Stanford University School of Medicine, Stanford, CA, 94305, USA.
*** Corresponding author. Department of Bioengineering, Faculty of Engineering, Ege University, 35100, Izmir, Turkey.
E-mail addresses: ozlem.yesil.celiktas@ege.edu.tr (O. Yesil-Celiktas), ebimsv@stanford.edu, ebi.mostafavi@gmail.com (E. Mostafavi), aozturk@istinye.edu.tr, aycabal@gmail.com (A. Bal-Öztürk).

https://doi.org/10.1016/j.bios.2023.115100
Received 16 October 2022; Received in revised form 7 January 2023; Accepted 22 January 2023
Available online 24 January 2023

stress from fluidic flow have been previously discussed as critical brain-on-a-chip (BoC) features (Amirifar et al., 2022; Bang et al., 2021), where BoC is being examined as a substitute for typical *in vitro* techniques and animal models (Aazmi et al., 2022; Lu et al., 2022). BoC is more accurate in predicting human-individual clinical effects than conventional preclinical prototypes (Jagtiani et al., 2022) and is a promising tool for disease modeling, drug testing, and personalized therapy (Ingber, 2022; Subia et al., 2021). These platforms also provide advantages such as rapid and affordable production procedures, design flexibility, and reduce the use of chemicals and precious cells (Haeberle and Zengerle, 2007; Mark et al., 2010).

Sensors aid in evaluating the stability of BoC and molecular transports by providing accurate data sampling, real-time detection, and/or suitable imaging (Azimzadeh et al., 2021; Liang and Yoon, 2021; Perestrelo et al., 2015). Recent microfluidic and sensor advancements may enable us to screen and simulate BoC physiological activities on a single platform, clearing gaps in *in vitro* BoC models (Liang and Yoon, 2021; Wang et al., 2020). Furthermore, interdependence, minimally invasive detection of blood-based biomarkers, simplicity, cost-effectiveness, early diagnosis with low concentration, and short time using disposable microfluidic platform (DμP) compared to commercial ELISA kit could offer exciting opportunities to improve the quality of life for patients (de Oliveira et al., 2020b).

Optical, mechanical, and electrochemical sensors can potentially be used with BoC models (Fuchs et al., 2021; Liang and Yoon, 2021; Strakosas et al., 2015). Color, absorbance, reflectance, and fluorescence are measured by optical sensors and converted into useable electrical signals (Chanda and Balamurali, 2021; Werner et al., 2021). Surface plasmon resonance (SPR) is another optical sensor that detects plasmon light wave changes on a metal surface through which a liquid sample flows (Homola et al., 2005; Piliarik et al., 2009). Optical sensors also direct fluorescence excitation (Dostálek et al., 2005), which has been miniaturized and incorporated into microfluidic devices (Chen et al., 2020; Wang and Fan, 2016). Mechanical sensors can measure surface stress or oscillation frequency to monitor mass deposition on a surface (Chen et al., 1995; Ricco and Martin, 1991). Also, these sensors can aid in accurate data collection, real-time detection, and/or suitable imaging (Liang and Yoon, 2021; Prodanov and Delbeke, 2016; Zhao et al., 2021). The surface-stress sensor uses a cantilever to monitor changes in deflection caused by molecular binding (Butt, 1996; Moulin et al., 2000). By observing how long a molecule takes to complete a cycle of dynamic oscillation at a fixed resonance frequency, the oscillation sensor may infer the strength of a molecule's binding (Eom et al., 2011; Subramanian et al., 2018). Electrochemical sensors have been differentiated into amperometric, potentiometric, conductometric, and impedimetric forms (Blanco-López et al., 2004; Mollarasouli et al., 2019). Amperometric sensors are used in glucose monitoring to quantify the changes in electronic current at a constant affected potential due to an enzyme-catalyzed reaction (Heller and Feldman, 2008; Touhami, 2014). Ion concentrations can be measured across electrodes using a potentiometric sensor (Mousavi et al., 2018). Under direct current, molecules that stick to the surface change the conductance, measured by a conductometric sensor. Impedimetric sensors are more regulated than other electrochemical sensors since they can specify more evidence of molecular binding without requiring bioreceptors like enzymes or antibodies (Grieshaber et al., 2008; Janata, 2009), which could be used to disrupt barrier integrity and induce BoC protein expression (Pediaditakis et al., 2021a; Vatine et al., 2019).

By adding (bio)sensors, the settings of BoC models can be fully measured and more accurate data can be collected. For translation to the clinic, incorporating biosensors into BoC has been discussed with challenges and limitations of biosensors combined with BoC platforms. Although sensor and biosensor combinations on BoC models are still in progress, some drug screening and testing studies have been demonstrated. More progressive technologies can be also introduced, resulting in automation, less effort, and improved stability (Ferrari et al., 2020; Rothbauer and Ertl, 2020; Zhu et al., 2021).

This review sums up the current design and basic biosensory capabilities of experimental models of BoC. We discussed how advanced biosensing technologies could be integrated with BoC systems. Future perspectives on how novel approaches will automate assays and improve point-of-care (PoC) diagnostics and accurate quantitative analyses is provided. We also address key challenges providing opportunities for clinical translation of BoC in neurodegenerative disorders, including eliminating electrode surface contamination, monitoring complex biofluids, and the signal reading, and adoption of PoC and BoC in personalized medicine diagnostic platforms.

2. Design principles: an overview

Recently, BoC models increasingly are being developed for clinical use. However, realization of the design specifications of a brain-specific microenvironment requires an understanding of the complexity and challenges of the brain, including microenvironment (native ECM of the brain, mechanical forces, physiochemical features, etc.), cellular components, different regions, subunits, interactions with other organs, and advanced functionality (Bang et al., 2019; Maoz, 2021). Over the last decade, BoC models integrating multiple properties of the brain have been proposed to investigate the BBB models (Oddo et al., 2019; Partyka et al., 2017), compartmentalized neural models (Fantuzzo et al., 2017; Taylor et al., 2005), interactions among neurons (Kilic et al., 2016), functional neuronal networks (Chwalek et al., 2015), and pathological models (Cavaliere et al., 2017; Fan et al., 2016; Gao et al. 2019). In this section, we examine technical issues and standard device designs and their uses.

2.1. General technical design considerations

The selection of chip material relies on such factors as gas solubility and permeability (especially O_2 and CO_2), fabrication method, functionality of the final device and biocompatibility (Leung et al., 2022). Poly(dimethylsiloxane) (PDMS), poly(methyl methacrylate) (PMMA), polystyrene, polycarbonate, and cyclic olefin copolymers are common materials used to make BoC platforms (Amirifar et al., 2022; Leung et al., 2022; Nielsen et al., 2019). Amongst them, PDMS is one of the most widely utilized materials for BoC applications due to its cost-effectiveness, biocompatibility, optical transparency, gas permeability, ability to generate high-resolution structures, and rapid curing (Maoz, 2021; Shirure and George, 2017). PDMS' flexibility permits the mechanical stimulation of cells (Huh et al., 2010), but its hydrophobicity and bioinertness result in reduced cellular adhesion (Carter et al., 2020; Gonçalves et al., 2022). Due to its hydrophobicity, PDMS adsorbs hydrophobic compounds such as drugs and neurotransmitters, affecting experimental outcomes (Gokaltun et al., 2017; Shirure and George, 2017). The PDMS surface treated with bovine serum albumin avoids the adsorption of large hydrophobic molecules (Ostuni et al., 2000) and the PDMS chamber coated with proteins or other compounds enhances cell adhesion. To produce a BBB model, PDMS was coated with laminin for the 'brain side' and fibronectin and collagen-IV for the 'blood side' to enhance cellular adhesion and differentiation (Vatine et al., 2019).

To fabricate microfluidic chips, BoC uses standard microfabrication techniques that include soft-lithography, photo-lithography laser-based patterning, and injection molding and casting (Gale et al., 2018; Lu et al., 2022; Mofazzal Jahromi et al., 2019). Yet making a functional BoC can be expensive and slow because microfabrication requires extra steps to add features like bio-models, sensors, and stimulus-loading elements that recreate the native brain tissue (Rodrigues et al., 2020; Yang et al., 2017). Reproducibility is vital for the fabrication of BoC platforms because even seemingly negligible variations in the process potentially lead to alterations at cellular and subcellular levels (Amirifar et al., 2022).

Static and dynamic culture conditions are generally used in

microfluidic systems (Arandian et al., 2019). An entirely static culture model cannot meet BoC platform requirements due to inadequate molecule exchange. Appropriate flow type and flow rate for media perfusion through the BoC device maintains a concentration gradient for nutrient and waste transport and provides the proper shear stress level induced by flow over a tissue surface; excessive shear stress makes it hard for neurons to stick together and live. Park et al. reported that 0.1–0.3 μL/min flow rate in a microfluidic system, similar to the interstitial flow rate in the brain, can enhance the neural progenitor cells' differentiation into neurons (Park et al., 2015). The brain comprises many sites that make specific interconnections for the generation of neurons, axons, synapses, and dendrites; as a result, numerous compartmentalized microfluidic co-culture models, including ordered physiological connections of neurons, have been introduced to investigate brain development, degeneration, and diseases (Zheng et al., 2016). Optimizing microchannel dimensions between each chamber creates neuronal extensions by maintaining separation between different cell types. A microfluidic device with a pattern of somal and axonal compartments connected by microgrooves was developed for the direction and isolation of CNS axons, biochemical analyses of axonal fractions, and localized treatments of axons and somata (Taylor et al., 2005). Peyrin et al. made a microfluidic platform that uses different types of neurons in separate chambers connected asymmetrically by funnel-shaped microchannels to make oriented neuronal networks (Peyrin et al., 2011). To investigate the formation of synapses and neurocircuits, Fantuzzo et al. recently created a compartmentalized microfluidic device with a large central chamber and twelve separate smaller chambers, including different human-derived neuronal subtypes (Fantuzzo et al., 2017).

Hydrogel-based materials have enormous potential to be used as ECM substrates due to their biomimicry and biocompatibility. The selection of appropriate ECM substrate material is vital to introduce a scaffold for cell adhesion. Chwalek et al. designed a model to realize the layered structure of the brain's cerebral cortex; neurons are seeded as the outer layer in a donut-shaped porous silk sponge and a collagen-filled structure, including robust neuronal protrusions, is generated as the inner layer, creating neural networks (Chwalek et al., 2015). Hydrogels can also be designed to meet the mechanical requirements of neural cells. It is well known that soft hydrogels can mimic brain elasticity (0.1–1 kPa) (Flanagan et al., 2002). Engler et al. have shown that human mesenchymal stem cells can differentiate into neurons following seeding on soft polyacrylamide gels with elastic moduli between 0.1 and 1 kPa (Engler et al., 2006). Banerjee et al. reported that neural stem cells (NSCs) encapsulated in 3D alginate hydrogels with a modulus of about 180 Pa accelerated neuronal differentiation (Banerjee et al., 2009).

The most crucial issue for *in vitro* model design is replicating the desired organ using appropriate cell types from suitable cell sources. Human-originated cells such as primary cells, immortalized cell lines, stem cells, and their differentiated progenies could be used in BoC platforms instead of animal-originated cells, which are weak in realizing human functionality and complexity (Ahadian et al., 2018; Zheng et al., 2016). Stem cells such as NSCs, induced pluripotent stem cells (iPSCs), and embryonic stem cells (ESCs) could be able to differentiate into many neural cells, including astrocytes (ASTs), oligodendrocytes and neurons. The formation of BoC models using stem cells could benefit drug-related applications or our understanding of the mechanism of neurodegenerative diseases (Adegbola et al., 2017; Alvarez et al., 2012; De Filippis et al., 2017; Mofazzal Jahromi et al., 2019). The human brain could be precisely realized in terms of structure and physiology using human iPSCs-based systems; hence, these cells could also be potentially used to elucidate brain development and neurodegenerative diseases. Human iPSCs-derived neural cells could be used to reconstruct the human neural system based on the molecular, cellular, and structural levels in a dynamic model (Koo et al., 2018; Mofazzal Jahromi et al., 2019; Qian et al., 2018; Vitrac and Cloëz-Tayarani, 2018). To study the interaction between different neuronal populations, Dauth et al. developed a multiregional BoC, composed of three separated cell populations isolated from the prefrontal cortex, hippocampus and amygdala that are connected by axons. Neurons derived from different brain areas showed unique behaviors *in vitro* (Dauth et al., 2017). In a recent study, Brofiga et al. studied *in vitro* heterogeneous interconnected neuronal networks consisting of cortical and hippocampal neurons by using a polymeric structure coupled to Micro-Electrode Arrays; here, hippocampal neurons significantly reflected inhibitory connections, though cortical neurons mostly made intrapopulation connections. Notably, topological characteristics supported network formation and maturation (Brofiga et al., 2022). Harberts et al. recently utilized direct laser writing to develop BoC-applicable 3D scaffolds and cultured human iPSC-derived midbrain dopaminergic neurons on these scaffolds. Their scaffolds comprise 24 elevated chambers connected by freestanding microchannels with designed neuronal network topology. This study gave BoC studies a new way of looking at how the brain works from a functional point of view (Harberts et al., 2020).

In vitro, 2D and 3D cellular models are widely used in BoC platforms to study the physiological and pathological functions of the CNS. Initial studies focused on utilizing 2D monolayer cellular models to separate the axon from a neuron's soma to evaluate its features or its regeneration following axotomy (Taylor et al., 2005; Tong et al., 2015). Later, several studies investigated drug efficacy or side effects (Mofazzal Jahromi et al., 2019). Nevertheless, 2D models can not mimic 3D native tissue architecture nor provide the capability to evaluate drug responses (Hoarau-Véchot et al., 2018; Mofazzal Jahromi et al., 2019). Studies indicate that instead, 3D bioprinted constructs, spheroids, organoids and microfabricated organ-on-a-chip (OoC) platforms present favorable alternatives to assess the efficacy and toxicity of drugs or realize neural systems in 3D models (Harberts et al., 2020; Ravi et al., 2015; Vinci et al., 2012). Spheroids and cell aggregates use scaffold-free approaches where cell aggregates spontaneously accumulate ECM. Organoids are the most beneficial models to mimic complex brain tissue. They are formed from aggregated stem cells incubated for an extended period to differentiate cells (Bang et al., 2021; Park et al., 2019a). The stem cells can be aggregated without ECM components, but organelles and matrix components make additional cues available. Eiraku et al. utilized Matrigel to present physicochemical cues, and their technique has been widely adopted in various studies (Eiraku et al., 2011). Many studies have reported region-specific brain organoids, including cerebellar (Muguruma et al., 2015), cerebral cortex (Paşca et al., 2015; Xiang et al., 2017), forebrain (Krefft et al., 2018), midbrain (Jo et al., 2016; Monzel et al., 2017) and hypothalamic organoids (Qian et al., 2016). Despite their power, brain organoid models have critical limitations. They present variable constructs with lack of control. In addition, for the study of neural network biological activities, the precise location of different neural cells is difficult to predict. In general, evaluating the genetic and biochemical properties of cells seeded in the 3D cell culture models is challenging. These models are also incapable of determining cellular tension and fluid stress (Amirifar et al., 2022; Mofazzal Jahromi et al., 2019) and inadequate oxygen and nutrient diffusion lead to devascularization and necrotic cell nuclei. Strategies have been demonstrated to overcome current challenges in brain organoids. Shi et al. introduced a vascularized organoid using cortical cell types and a vascular structure and differentiated and matured them for up to 200 days under optimized culture conditions. They demonstrated that in the grafts, after organoid transplant, functional blood vessels enhanced cell survival in the mouse S1 cortex (Shi et al., 2020).

2.2. Model designs

2.2.1. Models to mimic brain physiology

Recent advances in the development of OoC devices have led to studies of brain cell and physiology functions. Though brain tissue's complexity complicates the studies, considerable research exists on neuronal migration, neurite and axon formation, synapses, glial cells,

cell-cell communication, etc. Xu et al. introduced a microfluidic device incorporating Matrigel cylinder arrays with precisely controlled 3D diffusion to generate molecular gradients of varying steepness to investigate the effect of gradient steepness in neuronal chemotaxis. Multiple three-dimensional (3D) neuron cultures were created by seeding primary neurons on the hydrogel. Using this method, the cause of the chemotactic effect of semaphorin3A (Sema3A) was revealed to be serine/threonine kinase-11 and glycogen synthase kinase-3 signaling pathways that were involved in chemotactic regulation of repellence of neurite and neuronal migration (Xu et al., 2018). To study axon guidance and growth dynamics, Bhattacharjee et al. cultured primary neurons longterm to produce a large-scale 16 × 64 (1024-chamber) microfluidic gradient generator array. Chambers containing a single neuron were monitored and data was collected from approximately 150-250 neurons per device, producing statistically rich data sets. Hippocampal axon routing due to a netrin-1 gradient was found to be attractive at higher concentrations and repulsive at lower concentrations, depending on the concentration. The growth cone rotation was affected by the gradient's angle of incidence. This platform can be used to study the role of morphogen and chemokine gradients in axonal guidance, cellular migration, differentiation and immune response (Bhattacharjee and Folch, 2017).

Recently, Brofiga et al. developed the cortical-hippocampal and cortical-thalamic circuits using two PDMS masks paired with microelectrode arrays to study effect of thalamic and hippocampal inputs on cortical activity patterns. Distinct effects of thalamic and hippocampal activity regulated the spike and burst dynamics of the co-cultured cortical cells. Moreover, the cortical-hippocampal circuits exhibited a redistribution of the strongest connections, both excitatory and inhibitory, whereas the cortical-thalamic circuits exhibited a remarkable increase in inhibitory connections (Brofiga et al., 2021). Ndyabawe et al. introduced a multi-compartment platform for modelling neurospheres and accurate specification of neural stem cell fate into multiple neuronal phenotypes networks. This design was validated by the simultaneous specification of human neural stem cells to dopaminergic and GABAergic neurons in different compartments of the device. The neurospheres generated unbounded intact neuronal circuits between the neurosphere arrays in all compartments of the device. Their device could be beneficial to generate multiple neural conduction circuits to realize functional connectivity between specific human brain regions (Ndyabawe et al., 2020). Tong et al. used an open chamber microfluidic device integrated Matrigel as 3D scaffold. Their system provided the evolution of neuron-neuron communication networks wherein electrical stimulation or the unilateral presence of agonists to one compartment enabled the activation of neurons in the adjacent compartment. They also reported one-way communication between separate populations of cultures containing human forebrain and midbrain dopaminergic neurons (Tong et al., 2021). Kim et al. proposed an axonal guidance platform using a microelectrode array incorporated microfluidic chip including two chambers and a bridge microchannel to separate and guide the axons. NSCs were greatly differentiated into neural cells with electrical stimulation and the electrical stimulation and neurotrophic factor exhibited a synergic effect on axonal outgrowth (Kim et al., 2022). Spijkers et al. developed a compartmentalized 3D neurite outgrowth model and cultured iPSC-derived motor neurons in a gel as matrix. Somata and dendrites remained mainly in the somal compartment, but axons elongated to an adjacent layer of gel. Moreover, highly reproducible dose-dependent axonal outgrowth was shown to respond to vincristine as chemotherapeutic drug (Spijkers et al., 2021). De Vitis et al. purposed a three-compartment microfluidic system to culture three different cell populations in separate chambers to modulate cell migration, neurite guidance, and cell differentiation in the chip. They found that the optimal geometrical features of device and microfluidic setups supported higher adhesion and proliferation of neuron-like human cells, enabled migration of neuron and Schwann cells between different compartments. In addition, it is possible to differentiation of neuron like human cells and primary rat Schwann cells to specific phenotypes (De Vitis et al., 2021).

Shi et al. designed a platform to co-culture CNS neurons and glia using a vertically-layered chamber and a four-chamber setup equipped with pressure-enabled valve barriers to control communication between cell types. They provided dynamic visualizations of neuronal interactions (synapse development), co-culture of glia and neurons at close range (~50–100 μm) and differential transfection of neuronal populations. Communication between neurons and glia was reported as vital to the generation and stability of synapses (Shi et al., 2013). Yang et al. designed a compartmentalized microfluidic platform to allow neuron and oligodendrocyte cell body separation and myelin sheath formation by electrical stimulation. A five-fold increase in the number of myelinated segments/mm^2 was achieved in the presence of electrical stimulation of dorsal root ganglia compared to unstimulated controls (Yang et al., 2012).

2.2.2. BBB models

The BBB is a dynamic and highly selective physiological barrier between the systemic blood circulation and the CNS (Park et al., 2019b). It consists of brain microvascular endothelial cells (BMECs), pericytes, and ASTs. BMECs are the most critical BBB component, presenting a physical barrier based on complex, tight junctions. Pericytes, ASTs, basement membranes, and the ECM generate a microenvironment that maintains the integrity of the BBB (Lecuyer et al., 2016; Oddo et al., 2019). BBB-on-a-chip models could be employed to evaluate the BBB pathology based on many neurodegenerative diseases associated with stroke, vascular malformations, AD, multiple sclerosis, and tumors (Herland et al., 2016; Phan et al., 2017). For an ideal BBB model, native tissue should realize 3D vascular architecture of BMECs, cell-cell interactions, shear stress on BMECs due to flow, and permeability of basal membrane (Oddo et al., 2019). To date, models have realized the co-culture of related cells and shear stress applied to the BBB, but to precisely mimic the BBB requires biomaterial with a thickness of approximately 100 nm meeting such parameters as homeostasis, tissue maintenance, cell differentiation, and cell structural support (Nag, 2003; Oddo et al., 2019; Partyka et al., 2017). Strategies to recreate the BBB include sandwich structure design, parallel structure design and 3D tubular structure design. As a less common strategy, the vasculogenesis model has also been used in BBB systems to realize microvessels de novo (Amirifar et al., 2022) (Fig. 1). The sandwich design uses two PDMS microchannels (upper and lower) separated by a porous membrane such as a polycarbonate membrane with 0.2–3 μm pore diameter. The upper channel can be used to grow BMECs, and the lower channel can be used to produce pericytes and ASTs. This design's shortcomings include cell-cell contact inhibition, cell seeding variations and low membrane transparency which prevents accurate imaging (Maoz et al., 2018; Oddo et al., 2019; Sellgren et al., 2015). The parallel design uses PDMS microstructures such as a membrane horizontally separating two aligned microchannels (Amirifar et al., 2022). This design provides limited cell-cell interaction and sub-optimal imaging and PDMS membrane is about 50 μm thicker than that of the human BBB (about 100 nm) (Prabhakarpandian et al., 2013). In the 3D tubular structure design, cylindrical microchannels are used to achieve a consistent, continuous flow and uniform shear stress along the inner walls of the microchannels. Partyka et al. engineered a microfluidic device with a vessel-like structure to apply controlled flow to a co-culture of cerebral endothelial cells and ASTs-laden 3D hydrogels where the blood flow revealed mechanical stress (shear stress and cyclic stretch) regulating the barrier function by controlling transport across and along cerebral microvasculature walls (Partyka et al., 2017). Finally, vasculogenesis design has been presented as an advanced strategy to reconstruct microvessels de novo in BBB systems (Oddo et al., 2019). Bang et al. developed a system of dual microchannels for BMECs and neural cells separated by a fibrin hydrogel and supplemented by different media types to separate cell types. BMECs created vascular-like networks

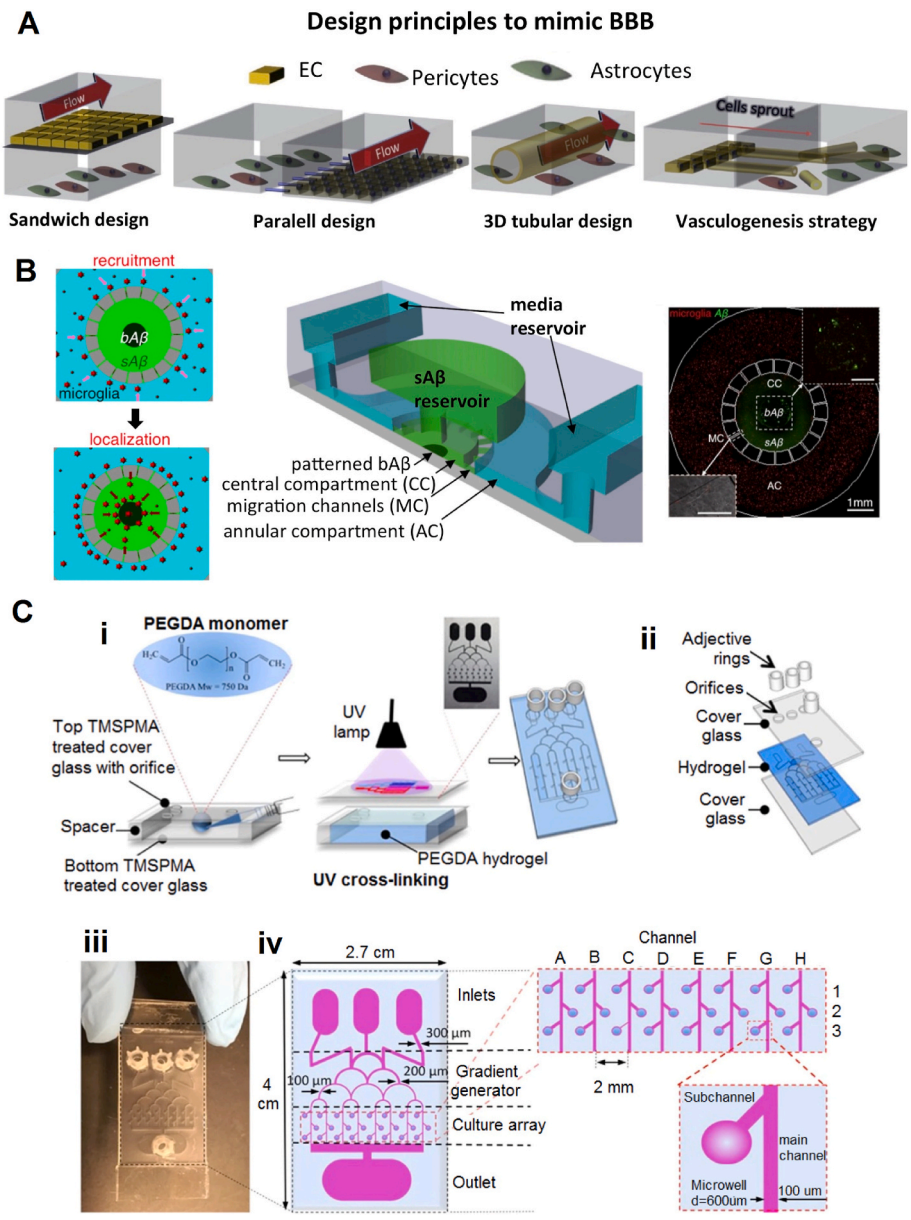

Fig. 1. (A) Design strategies for BBB models, including sandwich design, parallel design, 3D tubular structure design, and vasculogenesis. Reprinted with permission from (Oddo et al., 2019). **(B)** Microfluidic chemotaxis device mimicking pathological Aβ environments in AD brains. Reprinted with permission from (Cho et al., 2013). **(C)** Brain cancer chip design and fabrication. (i) Device including microchannels and microwells with inlet and outlet reservoirs above inlet and outlet orifices. (ii) Layers used for device generation. (iii) Photo of designed device. (iv) Christmas tree-shaped gradient generator channel system for the brain cancer chip. This device consists of an array of 24 separate culture chambers, three inlet reservoirs, and one outlet reservoir with a gradually decreased channel width from 300 to 100 μm. The sub-channels connect the microwells and the main channel to prevent captured cells from escaping the microwell. Reprinted with permission from (Fan et al., 2016).

within the fibrin hydrogel. This model cannot provide a complete neurovascular unit because of irregular branching but can achieve a functional model to evaluate endothelial cell and neuron interactions (Bang et al., 2017). The BBB assay on different microfluidic devices introduced mechanisms for an investigation with human brain microvascular endothelial cells (HBMECs), human brain vascular pericytes (HBVPs), and 3D human astrocytic (HAs) network. BBB models with various levels of shear stress were designed for the transepithelial/transendothelial electrical resistance (TEER) assay (Fig. 2).

2.2.3. *Disease models*

Alzheimer's disease (AD) is an age-related neurodegenerative disorder characterized by β-amyloid (Aβ) plaques and tau proteins (Yoon et al., 2021). Park et al. designed a microfluidic chip based on 3D neurospheroids derived from rat embryos; Aβ treatment with dynamic flow realized the flow rates of cerebrospinal fluid (CSF) and reduced the viability of neurospheroids, and dynamic flow improved Aβ expression (Liu et al., 2022; Park et al., 2015). Cho et al. developed a microfluidic chemotactic platform composed of a large central compartment, soluble Aβ patterns of surface-bound Aβ, and an annular compartment loaded with human microglia. Microglial responses to both long-lasting gradients of soluble Aβ and patterns of surface-bound Aβ were successfully quantified (Cho et al., 2013). Deleglise et al. presented a microfluidic device using primary cortical mouse neurons by compartmentalizing axon terminals from cortical neurons' cell bodies and applying Aβ peptides locally to each cellular compartment. Aβ application to the somatodendritic chamber caused axonal degeneration and a rapid loss of presynaptic connections in the cortex, but Aβ application to the chamber of extended axons had minimal effect. This system reportedly was useful in detecting early changes in AD (Deleglise et al., 2014). A recent study developed the AD-on-a-chip model; based on an NSCs spheroid-based biochip, it includes a multichannel system and microelectrode arrays (MEAs), allowing impedance analysis to detect network formation and degeneration in real time. In the presence of Aβ, synapse function and neurotransmitter-acetylcholine concentration were reduced, while reactive O_2 species accelerated. For network generation and neurite degeneration, real-time electric cell-substrate impedance--sensing data were comparable with biological data (Liu et al., 2022). Gao et al. designed a hippocampal neuronal network chip induced by Aβ oligomers to measure neuronal electrical activity and network

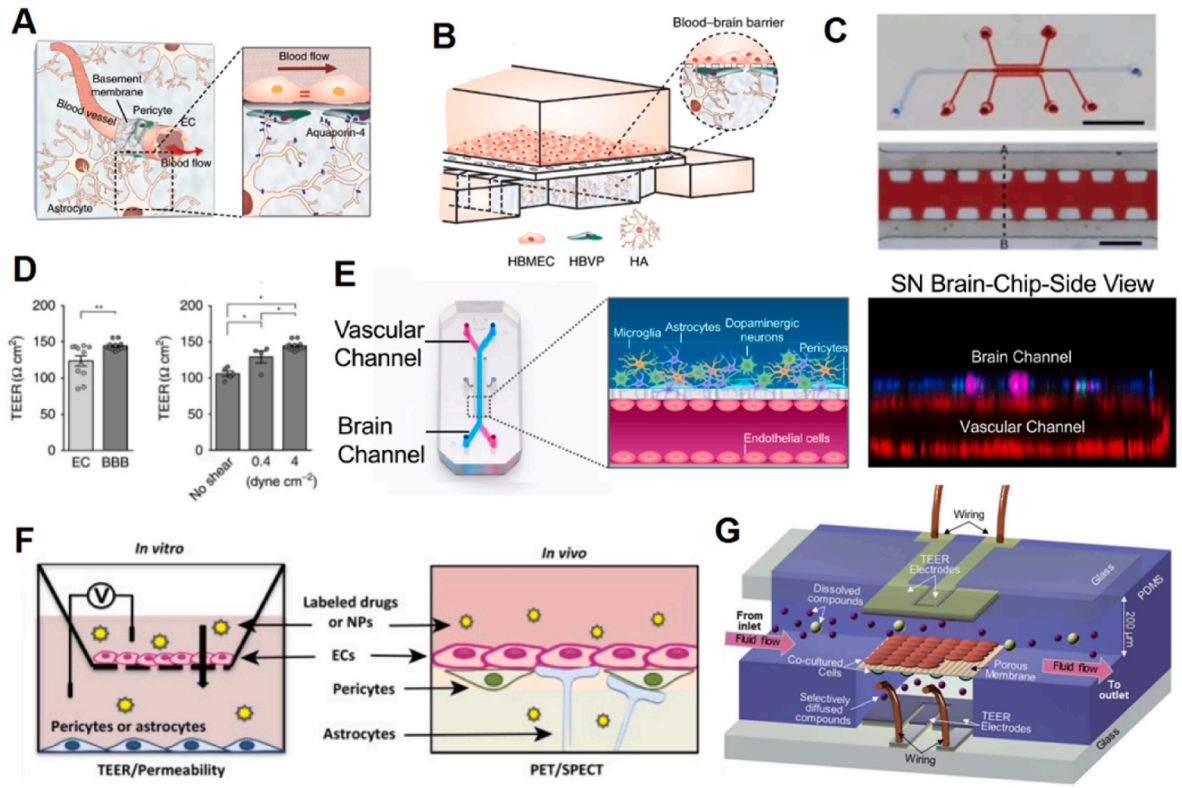

Fig. 2. Mechanisms for BBB assay on different microfluidic devices. **(A)** Schematic diagram for investigation of the mechanisms the BBB contains; ECs communicate with the blood vessels and endothelial monolayer covered by pericytes enables the expression of aquaporin-4 through ASTs that regulate the water inflow control and substances transporters across the membrane the bloodstream and brain. **(B)** Schematic description of the microfluidic system designed for BBB model with HBMECs, HBVPs), and 3D HAs network. **(C)** The microengineered BBB model of the microfluidic device is included upper channel (blue) and lower channels (red)) were compartmentalized with three parallel chambers using micropillars (scale bar = 500 μm). **(D)** The membrane between the upper and lower channels with an EC monolayer, ASTs, and pericytes was measured based on TEER (EC (n = 11), BBB (n = 12), **p < 0.01 by *t*-test). BBB models with various levels of shear stress were measured based on TEER (No shear (n = 5), 0.4 dyne/cm (n = 4), and 4 dyne/cm^2 (n = 12), *p < 0.05 by *t*-test). Reprinted with permission from (Ahn et al., 2020). **(E)** Schematic photo of the Substantia Nigra (SN) Brain-Chip of two microfluidic channels of microengineered chip with brain endothelial cells derived from iPSC. These cells were cultured seeding on the lower channel (vascular), and dopaminergic neurons differentiation of iPSC, microglia, primary brain ASTs, and pericytes seeding on the upper surface chamber (brain) with the 3D reconstruction of all cell lines in SN Brain-Chip. Reprinted with permission from (Pediaditakis et al., 2021b). **(F)** To evaluate the permeability transwell and TEER assay (*in vitro*) of EC cells covered on a porous surface and co-cultured with neurovascular unit cells such as HAs and HBVPs. For penetration measurements, solute or nanoparticles were labeled with radio- or fluorescent for measurements of apical (luminal) and basolateral (abluminal) sides. Furthermore, volt-ohm meters were used to measure TEER (*in vitro*). For permeability measurements of radiolabeled solutes in the brain (*in vivo*) were used imaging techniques such as SPECT and polyethylene terephthalate (PET) were used. Reprinted with permission from (Aday et al., 2016). **(G)** This μBBB system is a multi-layered device with two glass (perpendicular flow) channels, four PDMS substrates, and a porous polycarbonate membrane. Reprinted with permission from (Booth and Kim, 2012).

connectivity. After the treatment of Aβ oligomers, two firing patterns with distinct alterations from the interneurons and pyramidal neurons were monitored. The treatment of Aβ oligomers resulted in progressive network dysfunction. The disruption in neuronal network connectivity was validated through the spatial firing pattern map and channel cross-correlation (Gao et al. 2019). Altogether, microfluidic approaches employed for Aβ detection in plasma included IME sensors, droplets containing magnetic bead-based immunoassay, and enhancement of the detector's performance by dielectrophoretic force (Fig. 3).

Parkinson's disease (PD) is a slowly progressive neurodegenerative disease that affects the peripheral autonomic nervous system, leading to the loss of dopaminergic neurons and tremors, bradykinesia, and rigidity (Sharabi et al., 2021). Kane et al. developed a microfluidic platform for long-term maintenance and monitoring of patient-derived human neuroepithelial stem cells differentiating into dopaminergic neurons. They used calcium imaging to establish the electrophysiological activity of differentiated neurons and used an immunostaining assay to study the efficiency of the differentiation protocol. This automated platform facilitated long-term maintenance and made longitudinal optical detection of cellular parameters possible in real-time and end-point assays (Kane et al., 2019). Cavaliere et al. designed a platform with a single well or microfluidic chambers, providing a connection between the primary cultures of cortical neurons and ASTs. A-Synuclein (α-syn) is an important biomarker for monitoring the progression of PD; active transport of α-syn was determined between cells and any cell types, and α-syn uptake and spread from ASTs to neurons was found to result in neuronal death (Cavaliere et al., 2017).

Huntington's disease (HD) is a devastating and progressive neurodegenerative disorder with motor, psychiatric and cognitive features. HD occurs due to the repetition of a CAG trinucleotide in the Huntingtin gene (Bates et al., 2015). Virlogeux et al. introduced an OoC model to realize healthy and HD networks of presynaptic, synaptic, and postsynaptic neuronal compartments controlling the progression from axonal growth to synapse regulation. Different parts of the corticostriatal circuit exhibited major defects associated with the changing global synchronization of the network, including presynaptic dynamics, synaptic structure and conduction, and postsynaptic traffic and signaling. In particular, the genetic status of the presynaptic compartment was found to be necessary and sufficient to replace or repair the circuit (Virlogeux et al., 2018). The researchers employed this system to identify and validate new drug candidates for HD treatment (Virlogeux et al., 2021).

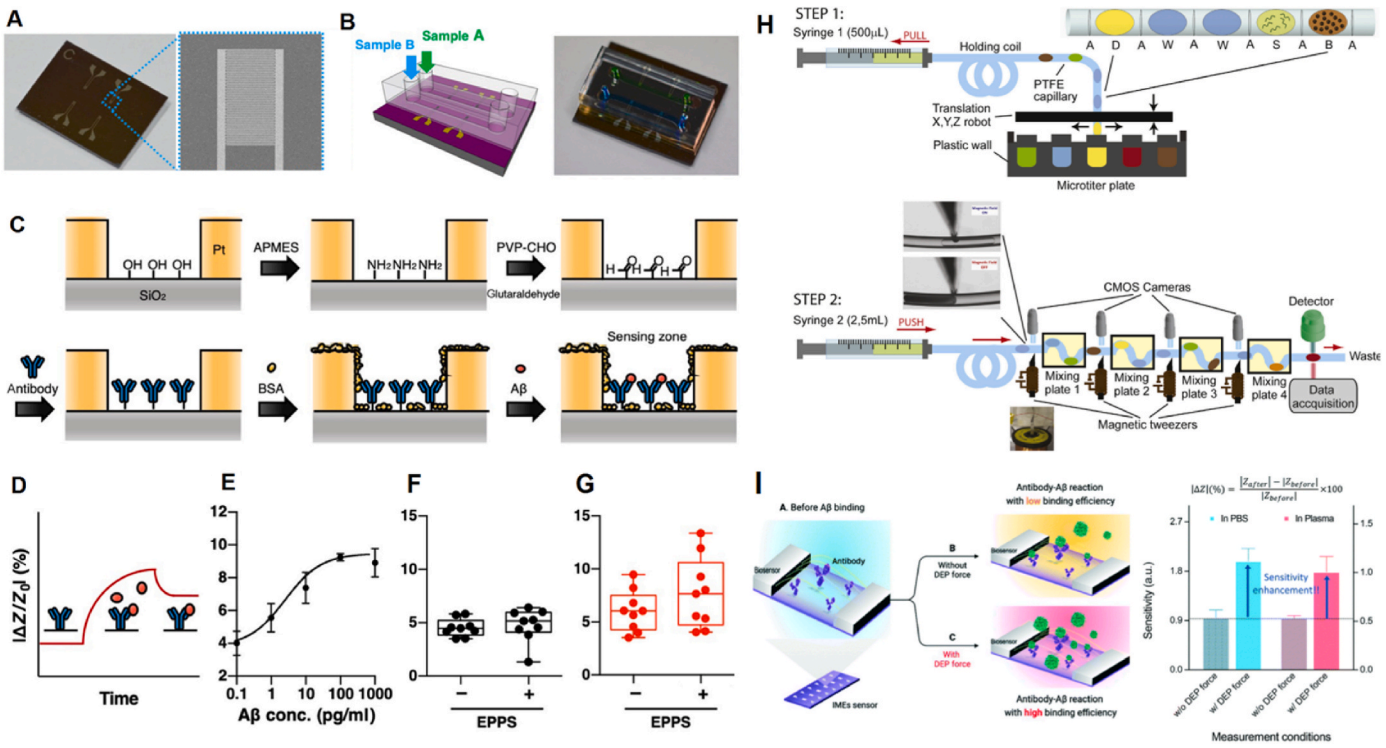

Fig. 3. Microfluidic approaches for Aβ detection **(A)** IME chip with four IME sensors and the enlarged photo of one IME pair. **(B)** Schematic illustration of IME sensor and PDMS chip incorporated with two microchannels on the chip to simultaneously load EPPS treated and nontreated that were injected with green and blue color solutions. **(C)** Sequential process of the IME sensor functionalized with the silicon dioxide (SiO_2) layer with 3-(ethoxydimethylsilyl)propylamine (APMES), Aβ antibody (6E10), polyvinyl pyrrolidone–aldehyde (PVP-CHO), and BSA were employed to Aβ detection with low concentrations in plasma. **(D)** IME sensors optimized by synthetic Aβ (1–42). Subsequent impedance changes (|ΔZ/Z0|, %) were measured by the interaction between Aβ and its antibody. **(E)** Logarithmical linear sensitivity to Aβ levels resulting in impedance changes of 4.0% (100 fg/mL), 5.5% (1 pg/mL), 7.3% (10 pg/mL), 9.2% (100 pg/mL), and 8.9% (1 ng/mL) (n = 5). **(F and G)** Analysis of WT mice samples Aβ levels [black dot, WT (n = 9); red dot, TG (n = 9)]; impedance changes with median values of 4.5%, 4.1% (lower quartile), and 4.6% (upper quartile). Analysis of TG mouse samples Aβ levels; impedance changes with the median value of 6.0%, 4.5% (lower quartile), and 6.7% (upper quartile) without and with EPPS treatment (n = 5). Two-tailed t-tests performed in the statistical analyses (*P < 0.05 and ***P < 0.001; nonsignificant analysis is not indicated). Reprinted with permission from (Kim et al., 2019). **(H)** Schematic illustration belonging to the operational protocol of the microfluidic devices for Aβ detection. Emulsion droplets contained magnetic beads and Aβ peptides encapsulated in fluorocarbon oil; droplets were pulled into the holding coil, collected using a PTFE capillary, and trapped in different reservoirs on a plastic wall plate. Then droplets containing magnetic beads were pushed parallel, downscaled with four synchronized magnetic tweezers, recirculated and moved unidirectionally. These droplets also are included with Aβ samples, fluorescence-detecting solutions, and washing buffer solutions in mixing plates. Finally, magnetic beads measured immunoassay using the detection droplet of the enzymatic substrate. Reprinted with permission from (Mai et al., 2018). **(I)** Schematic diagram of performance enhancement of the sensor by dielectrophoresis force. The efficiency of the antibody-Aβ reaction with high binding was enhanced 2-folds using the dielectrophoresis force. Reprinted with permission from (Kim et al., 2021).

To date, several types of research have focused on designing BoC systems to model tumorigenic microenvironments. In general, 2D cultures are utilized to investigate the cellular biology of tumors and the efficacy or toxicity of drugs (Unger et al., 2014). Nevertheless, 3D cell culture models could be beneficial in defining signaling molecules employed in cell-cell and cell-matrix interactions and new drug research (Lancaster et al., 2013; Mofazzal Jahromi et al., 2019; Tanner and Gottesman, 2015). Fan et al. developed a 3D brain cancer chip with glioblastoma multiforme, the most common and dangerous type of brain tumor. Using photo-lithography, they created a chip system with glioblastoma cell cultures on poly(ethylene) glycol diacrylate hydrogel to test Pitavastatin and Irinotecan in combination (Fan et al., 2016). Terrell-Hall et al. developed a BBB model in a microfluidic chip composed of a central basolateral compartment that included ASTs, pericytes, and neurons. An outer apical case included endothelial cells with perfusion comparable to physiological fluid flow. An array with 3 μm pores separates the chambers. Later, ASTs were replaced in the model by Met-1 metastatic murine breast cancer cells to create the blood-tumor barrier model. Shear stress, permeability, and efflux properties were similar to *in vivo* data (Terrell-Hall et al., 2017). Meanwhile, Oliver and colleagues developed a platform to quantitatively assay the dynamic phenotypes of breast cancer cells and brain metastases behavior (Fig. 4) (Oliver et al., 2019).

3. Basic biosensing principles

Despite their extraordinary features, BoC platforms have limited ability to accumulate real-time data about cells and their microenvironment in monitoring tissue development and their interaction with different stimuli (e.g., drug management) (Azizgolshani et al., 2021; Ferrari et al., 2020). Any instability in the physical environment of the culture can damage cells, so the features of the culture environment must be constantly monitored to ensure the physiological functioning of cultured cells within the OoC models (Khorsandi et al., 2021; Rezaei and Irannejad, 2019). Although there are numerous characterization approaches, such as different types of viability tests and quantification of biomarkers, to evaluate the cytotoxicity or functionality of therapeutic components, they still depend on ELISA or other off-chip analysis and imaging techniques and are usually limited by end-point tests. So, real-time monitoring of any change in BoC platforms is critical. An essential advancement has been integrating biosensors with BoC platforms (Caballero et al., 2017; Rudi and Kratz et al., 2019).

Biosensors are platforms capable of converting a biological or chemical reaction into measurable signals (Chadha et al., 2022; Kang

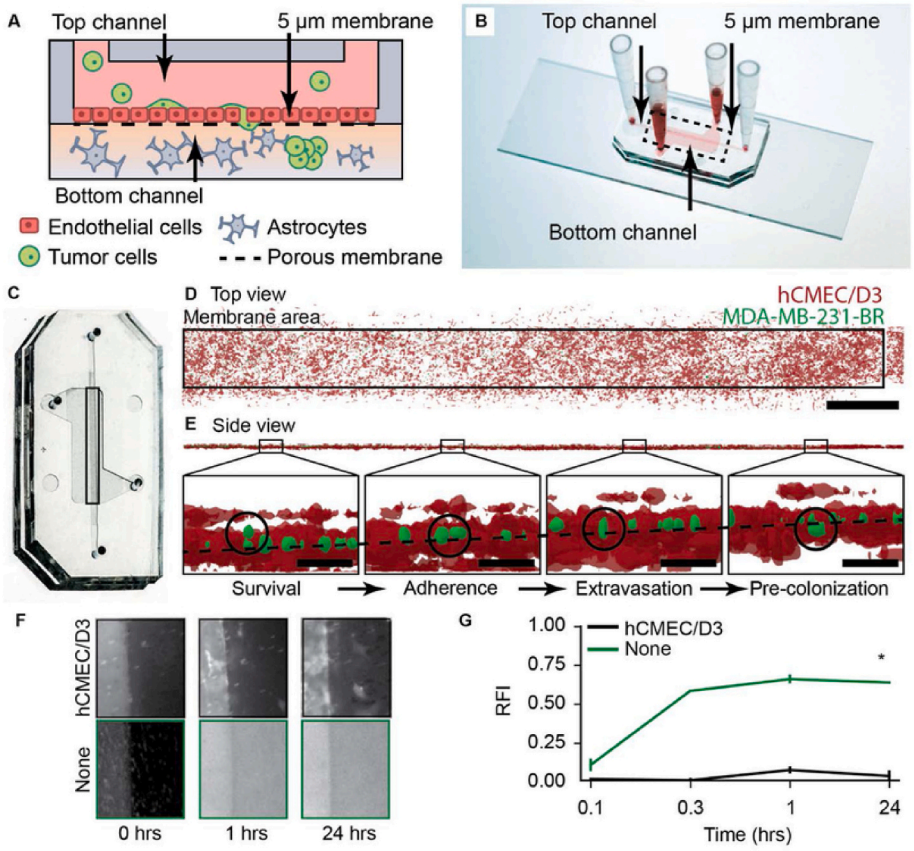

Fig. 4. A μBBNiche device designed to assay the process of brain metastatic. **(A)** Schematic rendering of a μBBN device. **(B)** Sections of the μBBNiche device with the top and bottom channels and porous membrane. **(C)** Confocal 3D rendered objects of μBBNiche device. The hCMEC/D3 endothelial layer in the μBBNiche device forms a barrier between the top and bottom channels. **(D)** Top view of the μBBNiche instrument (black rectangle) shows MDA-MB-231-BR cells post-seed 24 h top-down chamber (scale bar = 1000 μm). **(E)** Side view of the channel in μBBNiche system with insets cancer cells show various stages in metastatic cascade of traversing endothelium. The dashed line is stated with survival, pursued by adherence, then extravasation. In the end, pre-colonization is planned for the endothelium (black circles highlight representative cells) (scale bar = 200 μm). **(F)** μBBNiche system after adding 10 kDa FITC-Dextran; assessed with hCMEC/D3 cells (black boxes) and device without (green boxes) at the timeframes 0, 1, and 24 h. **(G)** Quantitative permeability measured after adding FITC-dextran in devices with and without the hCMEC/D3 layer over 24 h. Average values of three regions with n = 3 biological replicates. Error bars represent standard deviation (*$p < 0.05$). Reprinted with permission from (Oliver et al., 2019).

et al., 2022; Zare et al., 2021). They contain a bio-receptor, analyte, transducer, and detector (Qin et al., 2022). It is hoped that integrating these devices into the BoC systems can facilitate disease detection and treatment, halt disease progression and contribute to drug testing (Aleman et al., 2021; Mir et al., 2022; Xie et al., 2022). An AD model was fabricated to study network neurodegeneration mechanisms and different therapeutic methods that could be used in the disease. The model functioned based on the electrical activity of neurons and their network connections through multisite measurements (Gao et al. 2019).

BoC devices integrate different types of biosensors for monitoring the culture environment (such as dissolved O_2, temperature, and pH), cell activity, cell function (such as organ activity and barrier integrity) and respond to external stimulation factors like mechanical, electrical, and drugs (Fig. 5) (Zhu et al., 2021). Notable characteristics of this integration are high compatibility with microfluidic devices, high detection capacity, high sensitivity and minimal invasiveness (Kilic et al., 2018). BoC devices enable the fabrication of PoC devices for real-time detection and control of disease, even at home (Khorsandi et al. 2019, 2019zsoylu et al., 2022). Agostini and his coworkers manufactured a type of PoC biosensing chip for recognizing GFAP, a known biomarker for CNS diseases that include intracerebral hemorrhage, optical neuromyelitis, glioblastoma multiforme, multiple sclerosis, and traumatic brain injuries. A quartz-crystal-microbalance sensor within the chip worked based on the interaction of biomarkers and immobilized antibodies on its surface (Agostini et al., 2021).

So far, different types of biosensors have been incorporated into BoC platforms to monitor their various features (Table 1). We classify these biosensors according to their specific properties and their incorporation into the BoC systems for a particular detection.

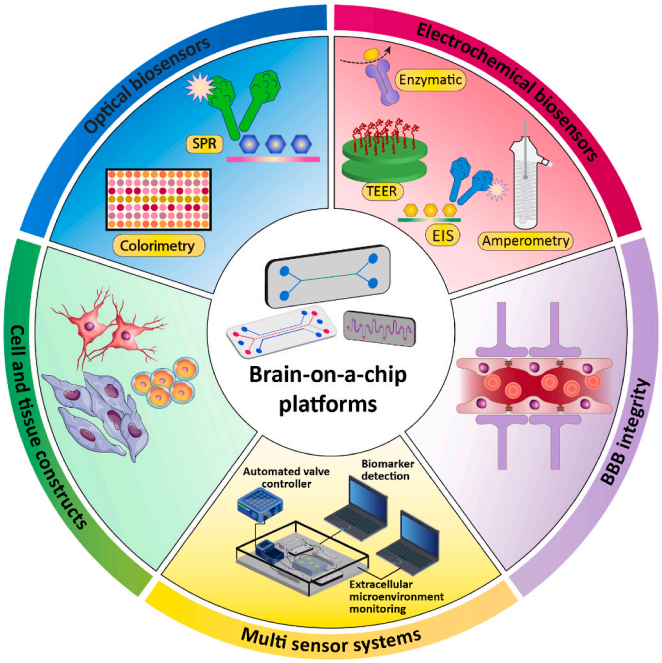

Fig. 5. Schematic of incorporation of different biosensors into BoC platforms. Biosensors are real-time detectors that work based on different detection methods including optical (like optical and surface plasmon resonance), electrochemical (amperometric, potentiometric, voltametric, etc.), electrical, and multi-detectors. They can be incorporated into brain-on-a-chip platforms for real-time monitoring of disease models.

Table 1
Analytical performance of BBB microfluidic devices.

Sensing mechanisms	Coupling methods	Analytes	Cell types/samples	Microfluidic materials	LOD	Refs
Electrical	Mass spectrometric	Neurotransmitters (dopamine, serotonin, aspartic acid, and glutamic acid)	PC-12 neuronal cells	PDMS, nano-electrospray Au electrode	42 Nm (DA), 49 Nm (5-HT), 8 nM (Asp), 32 nM (Glu)	(Li et al., 2016)
Electrical	AFM, FESEM	Aβ (1–42)	CSF	CNT film, metal-semiconductor field effect transistor structure, Au top gate, Si/SiO_2, Au, and Cr electrodes	1 pg/mL (Aβ (1–42))	(Oh et al., 2013)
Electrical	TEM, FM	α-syn	α-syn protein	Si oxide film, small unilamellar vesicles, 1,2-dioleoyl-sn-glycero-3-[phospho-L-serine], 1-palmitoyl-2-oleoyl-sn-glycero-3-phosphocholine	N/A	(Hu et al., 2016)
Electrical	SEM, FM, FITC	Human IgG, AD7c-NTP	Static tremors of neurodegenerative disease patients	*Morpho menelaus* wings up layer, SiO_2 nanoparticles	12 ng/mL (human IgG) and 4.5 ng/mL (AD7c-NTP)	(He et al., 2018)
Optical	Single-step magnetic-beads-based immunoassays	Aβ (1–40), Aβ (2–40), and Aβ (5–40)	CSF	Green LED, Si photodiode, custom-made lock-in amplifier	0.5–1 nM	(Mai et al., 2018)
Optical	FITC	Aβ (1–42)	Wild-type mouse plasma	300 nm thick uniform SiO_2, Pt electrodes, Ti layer, PDMS	100 fg/mL to 1 ng/mL	(Yoo et al.)
Optical	N/A	Aβ (1–42)	CSF	Si/SiO_2, dimethylacrylamide, N-acryloyloxy succiniester, 3-(trimethoxysilyl)propyl methacrylate	73.07 pg/mL (Aβ (1–42))	(Gagni et al., 2013)
Optical	AFM and X-ray photoemissive spectroscopy	Aβ (1–42)	CSF	Si wafer carboxylated alkyltrichlorosilane	300 ng/mL (66 nM)	(Ammar et al., 2013)
Optical	SEM imaging	Aβ (1–42), T-tau	CSF	Anodic aluminum oxide thin film, aluminum thin film, PDMS	7.8 pg/mL (Aβ (1–42)), 15.6 pg/mL (T-tau)	(Song et al., 2018)
Optical	SERS, AFM and SEM images, optical microscopy	NAA	Blood plasma (severe and mild TBI)	Sub-micrometer pillars, plasmon-active nanometric Au layer	0.021 pg/mL (0.12 pM) (NAA), 3.99 pg/mL (0.19 pM) (S100B), 3.35 pg/mL (0.02 pM) (GFAP)	(Rickard et al., 2020)
Optical	FM	PDGF-AA, GDNF, IGF-1, BDNF, FGF-2, BMP-4, IL-6, CNTF, NT-3 β-NGF	hiPSCs	PDMS-fabricated microchambers array, multiplexed *in situ* tagging array, SU-8 2100 (Microchem), 4-inch silicon wafer	20.4 pg/mL (GDNF), 18.0 pg/mL (PDGF-AA), 2.7 pg/mL (IL-6), 8.5 pg/mL (CNTF), 14.9 pg/mL (IGF-1), 23.3 pg/mL (BDNF), 12.0 pg/mL (FGF-2), 57.2 pg/mL (NT-3), 11.2 pg/mL (BMP-4), 39.1 pg/mL (β-NGF)	(Abdullah et al., 2020)
Electrochemical	Confocal fluorescent imaging	Dopamine homeostasis	SH-SY5Y cells	ITO WE, ITO counter/Pseudore RE	11.6 nM	(Yu et al., 2019)
Electrochemical	Computed tomography scan image	Glutamate, glucose, and lactate	Cortex (peri-lesion tissue)	PDMS, polyetheretherketone, Veroclear, ABS 3SP white	0.25 μM	(Samper et al., 2019)
Electrochemical	CV, EIS, chronoamperometry	Dopamine	SCF	SiO_2, Au, Ag, Cr adhesive layer, PDMS	0.1 nM	(Senel et al., 2020)
Electrochemical	WE geometry (circle, line, cross, star), CV	Dopamine	SH-SY5Y cells	ITO WE, ITO counter/pseudo-RE	30 nM	(Yu et al., 2016)
Electrochemical	SEM, EDX detector, AFM, CV	ADAM10	SCF	DμP, an array of 8 WE, CE, pseudo-RE, syringe pump, chromatographic injection valve, poly (diallyldimethylammonium chloride), AuNP film	0.35 fg/mL	(de Oliveira et al., 2020a)
Electrochemical	N/A	GFAP	CNS injuries	PET substrate, nitrocellulose, virgin wood, PMMA, pressure-sensitive adhesive sheets fibers	3 pg/mL and 39 mL pg/mm^2	(Salahandish et al., 2022)
Electrochemical	SEM, PET, Mini-Mental State Examination, Magnetic resonance imaging	Aβ (1–42)	AD patient plasma samples	SiO_2, Ti, the Pt electrodes, APMES, PVP-CHO, PDMS	0.1 pg/mL	(Kim et al., 2019)
Electrochemical	FESEM, AFM, X-ray photoelectron spectroscopy	Aβ	Human serum	Electrode materials (Ag/AgCl, nonpolarizable) and Au (polarizable), Cr and Au, micron-scale organic electrochemical transistor	100 zM	(Koklu et al., 2021)

3.1. Electrical biosensors

Electrical biosensors are based on an electrode modified with bio-recognition elements that detect the existence of a specific analyte by generating an electrical signal (Ansari and Malhotra, 2022; Dilgin et al., 2021). They can be classified into electrochemical or electronic sensors (Nadzirah et al., 2022). They can be incorporated simply into BoC models and demonstrate the extensive dynamic ranges with low detection limit (Rothbauer and Ertl, 2020; Zhu et al., 2021). Since the technical counterpart plays a crucial role in the development of a BoC, the equipment should allow extended recordings of the spontaneous activity brought on by the interactions of the ensembles as well as the delivery of electrical pulses in a secure environment (stimulus-evoked activity). In this regard, integrated microelectrode arrays (MEAs) are an accepted and effective means of interacting with the biological equivalent. MEAs function on combined physiological and electrical processes (Brofiga et al., 2021; Obien et al., 2015). The first 3D MEA effort was applied to brain slices in 1997. The cutting process results in accumulation of dead cell layers on the surface of brain tissues, so that coupling to planar electrodes is challenging. The need to comprehend information transmission within the 3D neural system has grown over time. To map the 3D electrophysiological activity, biocompatible and minimally intrusive technologies have been created. A platform was created by Soscia et al. in 2020 to measure the electrophysiological activity of three separate 3D cultures, simultaneously; each device featured 80 thin-film electrodes on 10 flexible polymer probes. A year later, Shin et al. created a device to collect information about the functional topological characteristics of the network; the device recorded the electrophysiological activity of *in vitro* 3D models. The device was also used in the AD-on-a-chip model for real-time assessment of the formation and degeneration of networks using impedance analysis; here, impedance electrodes were used to determine the effect of Aβ addition to the BoC model, and it was found that the presence of Aβ increased the impedance value due to neurite damage (Liu et al., 2022).

TEER-based biosensors are a type of electrical biosensor established to measure barrier integrity noninvasively. This sensor measures the tension in different cell growth and differentiation stages using electrical resistance across a monolayer of cells (Bednarek, 2022). Two electrodes (made of metal wires or patterned thin film electrodes) are mounted on both sides of the microfluidic channel; the voltage drop across them is measured for a square-wave low-frequency AC (Jain et al., 2020). The sensor can also determine whether a chi-square wave is fully formed or intact. TEER measurements integrated into BoC models could facilitate cell viability predictions and drug toxicity evaluation (Jeong et al., 2018; Khalid et al., 2020; Yu et al., 2020). TEER could also be used for rapid noninvasive detection of membrane permeability via measuring the electrical impedance across the cellular layer, as seen in study evaluating the effect of inflammatory stimuli conditions on the permeability of a BBB-on-a-chip model (Yu et al., 2020).

3.2. Electrochemical biosensors

Electrochemical biosensors are a subclass of electrical sensors that function based on direct conversion of a biological event into an electrical signal. The conversion uses a counter electrode (CE), a working electrode (WE), and a reference electrode (RE) (Ahadian et al., 2018; Lopes et al., 2022). One of the most exciting uses of these biosensors is in the structure of various BoCs. Biosensors can be functionalized and calibrated individually, then attached to the chip to measure in-situ analytes (Syama and Mohanan, 2021). They can be used to measure ion concentrations (pH acidification), O_2 (respiration), short-term reactive species, and molecules like glucose and lactate (energy metabolism) (Kavand et al., 2022).

According to the electrochemical reaction type, potentiometric, voltammetric, and amperometric biosensors have been introduced (Ahadian et al., 2018; Kavand et al., 2022). The potentiometric sensors react to analyte concentration variations using features like chemically modified electrodes, ion-selective membrane types, and ion-selective field-effect transistors (Lopes et al., 2022; Rezaei and Irannejad, 2019). In voltammetric and amperometric sensors, frequently used for measuring the metabolic markers and microenvironmental physical parameters of BoC platforms, detection is based on changes in the current value (Matthews et al., 2021; Zhu et al., 2021). Enzyme-based sensors integrated into the structure of BBB platforms have been used to monitor reactive oxygen (ROS) production. These biosensors function on the interaction between an enzyme (like superoxide dismutase or horseradish peroxidase) and a type of ROS molecule (like H_2O_2) that can be used to monitor neuroinflammation reactions (Mir et al., 2022). Conductance, impedance and capacitor-derived impedance are other electrochemical principles underlying the function of electrochemical biosensors (Rezaei and Irannejad, 2019). Incorporating enzymes (enzymatic biosensor); organic and inorganic mediators; aptamers; RNA; and molecularly imprinted polymers in the structure of these biosensors could improve their selectivity and accuracy for detection of a specific analyte, even when it is present only in low concentrations (Karimi-Maleh et al., 2020).

Electrochemical biosensors are divided into two functional types: sensors that measure metabolic activity (e.g., glucose or lactate, O_2, and pH with high time resolution) and sensors that measure biomarkers such as proteins, exosomes or other specific molecules (Kavand et al., 2022). An electrochemical biosensor detecting glutamate released from brain organoid ESCs was a novel method for identifying dynamic changes in neurotransmitter levels within hESC-derived cerebral organoids, which could be used to improve models for neurodevelopmental and neurological disorders (Nasr et al., 2018).

3.3. Optical biosensors

Optical biosensors function through an optical transducer system that converts biorecognition sensing element signals into optical signals (Damborský et al., 2016). Optical biosensors can be applied to the measurement of biological parameters using different features of light (resonance, reflection, polarization, and plasmon effect) and direct integration with microfluid. They are highly sensitive biosensors with long-lasting optical signals, low noise, and high time-resolution, eliminating the need for physical and electrical contact between the electrode and the detector in solution. Optical biosensors do not form an O_2 discharge zone at the electrode surface, so they are more practical at low O_2 levels (Kilic et al., 2018). Optical biosensors are categorized as labeled and unlabeled. Unlabeled biosensors function to generate the signal directly by interacting the analyzed material with the transducer. In contrast, in Labeled biosensors function apply a labeling agent, then measure the optical signal using such methods as colorimetry, fluorescence, luminosity, chemical illumination, SPR and amplified surface Raman scattering (SERS) (Khorablou et al., 2021). Colorimetric sensors such as pH, glucose, nicotinamide adenine dinucleotide, and 6-hydroxy dopamine are very popular in BoC platforms because they are simple and low-cost (Ahadian et al., 2018). Rickard et al. reported using a SERS-integrated optofluidic device for PoC detection of neurological biomarkers of severe traumatic brain injury (sTBI), such as N-acetylasparate (NAA) and GFAP. Their simple, non-invasive, affordable, reproducible and portable technology for neural trauma assay is intended for triage of traumatic brain injury (TBI) patients in clinical and prehospital settings. The main challenge associated with TBI-indicative biomarkers diagnostics is they are considerably lower in concentration than CSF due to the dilution of blood volume (Rickard et al., 2020).

Fluid-based biosensors are the most common and easily used optical biosensors. Photoluminescence biosensors have been incorporated into an O_2 sensor, detecting O_2 pressure using the quenching capability of O_2 (Mousavi Shaegh et al., 2016). Most fluorescence biosensors are coupled with lab-on-chip devices to detect biomarkers of different brain-related diseases; various biosensor-integrated chips are introduced according to

the interaction between the target molecule and a detecting compound that is intrinsically fluorescent or labeled with a fluorophore. The interaction between the molecules leads to the appearance of fluorescence via the Förster resonance energy transfer. Before the interaction between the analyte and its targeted compound interaction, no fluorescence is recorded due to the presence of a quenching agent; the interaction between the analyte and its target triggers structural change and the appearance of fluorescence (Khan and Song, 2020). Different BoC systems using this feature have been fabricated to detect neurodegenerative diseases and brain-related cancers and drug diffusion across the BBB (Ameri et al., 2020; Brazaca et al., 2020; Liang and Yoon, 2021; Song et al., 2020).

Due to their ease of integration, SPR and local surface plasmon resonance (LSPR) are extensively used in microfluidic instruments for bioassay. A beam of light trapped in metal nanoparticles or nanostructures smaller than the wavelength of light causes LSPR (Zhu et al., 2021). The sensitivity of SPR sensors can be enhanced by combining them with other technologies, such as nanohole arrays. These stimulate plasmons to produce excellent light transmission and are very sensitive to changes in surface refraction resulting from adhesion of biomolecules to the biosensor's surface (Nangare and Patil, 2022; Picciolini et al., 2018; Zhao et al., 2017; Zhu et al., 2021). Due to their extraordinary optical transmission, which can prevent the prism-coupling mechanism, nanohole arrays easily fit into the lens-free on-a-chip imaging setup, making them ideal candidates for miniaturization. This combination of SPR sensor and nanohole array was used for the highly sensitive and selective detection of cytokine sections from live cells (Liao et al., 2019).

3.4. Multi-sensors

A network of sensors detecting one element or various elements in communication led to the fabrication of multi-sensors. These exquisitely sensitive biosensors are used for highly accurate detection of an analyte (Liang and Yoon, 2021). As BoC platforms advance, it is critical to use integrated and multi-parameter sensors for automated and online monitoring of biochemical reactions; tissue metabolites; microenvironmental parameters (ie, O_2 and cytokines); and the extracellular environment (Ferrari et al., 2020). It is impossible to monitor these in an organ with a simple biosensor. Instead a combination of biosensors is needed. Thus, multi-sensors are ideal for monitoring multi-organ platforms (Ferrari et al., 2020).

4. BoC platforms incorporating advanced biosensing technologies

In disease modeling and personalized medicine, OoC systems have shown promise in predicting clinical outcomes. Still, these systems have limited in their ability to collect real-time data on diseased and healthy tissue environment just as their limited capability to simulate human pathophysiology in a biologically relevant manner. Single-time endpoint analyses (e.g., ELISA, cell viability, qPCR) evaluate cellular status and responses to certain chemical and mechanical stimuli, but understanding intracellular signaling pathways requires real-time and label-free analysis. To date in-situ integration of sensors is considered significant progress in tackling the technical drawback of such systems. To monitor the cellular microenvironment (e.g., pH, dissolved O_2) in the lung (Khalid et al., 2020), liver (Weltin et al., 2017), gut (Marrero et al., 2021), heart (Zhang et al., 2021), and BoC systems (Li et al., 2021; Liang and Yoon, 2021), several electrochemical (MEAs, impedance spectroscopy, TEER, etc.) and optical (e.g., SPR) sensors have been reported over the last decades. Advantages of the microfluidic devices include mimicry of electrophysiological natural media, low-cost, real-time monitoring, improved electrical recording *in vitro*, and adaptation to fluid complexity (Curto et al., 2017; Holloway et al., 2021). Meanwhile, machine intelligence and/or data-driven optimization involved in OoC technologies will significantly benefit microfluidic platforms. Development and modulation of more sophisticated microscopy, spectroscopy, and automated multi-sensing instrumentation is overcoming some of the challenges to detection of reactions on microchips (Galan et al., 2020).

Microphysiological systems based on sensing devices enable integrated monitoring platforms using impedance, TEER, and electrophysiological techniques. These systems allow continuous multiparametric data collection – over hours, not weeks – by monitoring cell media and cellular processes, including phenotype, cell metabolism, and growth (Holloway et al., 2021; Modena et al., 2018).

4.1. Monitoring BBB integrity with electrical sensors

The brain establishes physical interaction between the sensors and neural cells, allowing the transfer of information through the CNS (Yaldiz et al., 2022). The BBB is formed by endothelial cells interacting with brain perivascular cells such as pericytes, ASTs, microglia, etc. Its integrity protects neurons and other brain cells from disease-associated molecules (Fig. 6A). The tight intercellular junctions of brain endothelial cells within the BBB have high electrical resistance, maintaining selective permeability. Although freeze-fracture electron microscopy or paracellular tracer compounds (e.g., fluorescein isothiocyanate (FITC)-labeled dextrans, horseradish peroxidase) are widely used to control barrier integrity and permeability (Adriani et al., 2017; Partyka et al., 2017), the potential interference problems of the tracers limit their uses. Noninvasive and biocompatible TEER measurements are a widely accepted standard for continuous monitoring. More recently, they have become an emerging technology for BBB-on-a-chip platforms. Since TEER measurement requires a monolayer feature, these measurements in BBB-on-a-chip systems can also be regarded as 2D.

One step closer to *in vivo*, the cell-laden hydrogel layers and the continuous flow causing shear stress on cells within the BBB-on-a-chips can be considered critical differences from the transwells. It is challenging to monitor and record changes in membrane integrity using TEER due to the small dimensions of BBB-on-a-chip systems, but inserted electrodes/probes in the microfluidic channels have shown promise in such scenarios (Jeong et al., 2018; Motallebnejad et al., 2019; Ugolini et al., 2018; Yu et al., 2020). Still, electrode material characteristics, uneven current densities, minor variations in cell confluency and even geometry-related effects have a significant impact on TEER, continuing to challenge the assessment of barrier quality in OoC systems (Odijk et al., 2015). To cross-validate the differences in barrier function within the same device, Ahn et al. adopted the structure of BBB where the porous membrane was sandwiched between the upper, then lowered the PDMS layers supported by BMECs and by human ASTs. They then measured the TEER values of both monolayer BMECs and BBB model, including BMECs and 3D ASTs-laden hydrogels, via electrode wires inserted in the inlet and outlet of channel (Ahn et al., 2020). The researchers reported that as a result, hydrogel layer in the lower channel prevents the electrode coating and concluded the TEER might be affected by the uneven distribution of the potential across the membrane. Another issue reported with microfluidic-based platforms was due to the continuous flow and layer-by-layer 3D constructs; there was a lower standard of TEER values than transwells for the BBB (Wolff et al., 2015). Wang et al. developed a model with continuous tight junction and *in vivo*-like TEER values. They used primary rat astrocytes, smaller and less complex compared to their human counterparts. Although they asserted that BMECs respond to rat-sourced ASTs, they switched to human-sourced ASTs to create a complete human model for further development (Wang et al., 2017). Vatine et al. on the other hand, made a fully-humanized BBB-on-a-chip platform, combining OoC technology with human iPSC-derived brain microvascular endothelial-like cells, ASTs and neurons (Vatine et al., 2019) (Fig. 6B). Their iPSC-based BBB-on-a-chip model, in which Au electrodes were integrated into the platform, obtained physiologically relevant TEER values even under high shear stress conditions. Using iPSC-BMECs with BBB-on-a-chips,

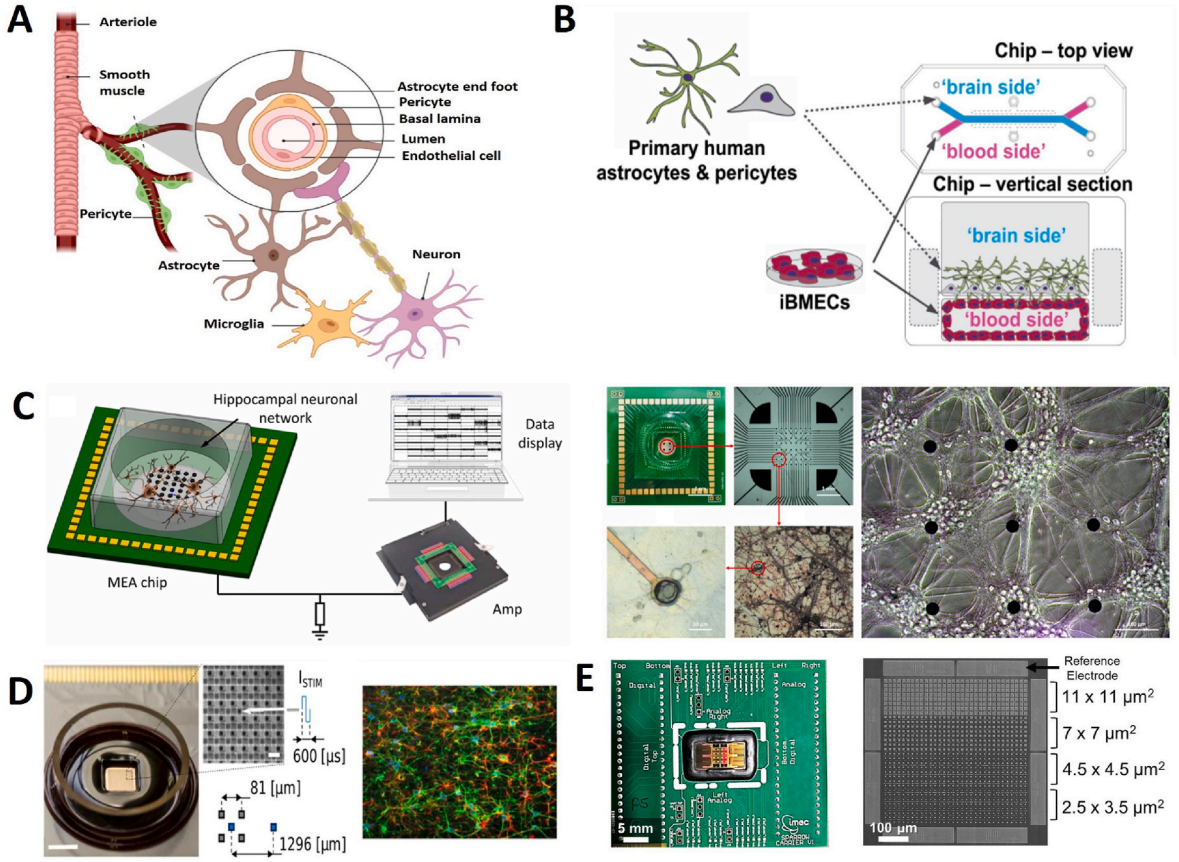

Fig. 6. Representative *in vitro* platforms designed for real-time monitoring of various parts of CNS. **(A)** An illustrated explanation of the BBB system. Adapted from "Neuron Anatomy" and "Brain Vascular System" BioRender.com (2022). **(B)** Human iPSC-based BBB-on-a-chip platform integrated with gold (Au) electrodes to measure real-time TEER values. Reprinted with permission from (Vatine et al., 2019). **(C)** Schematics of the PDMS assembled MEAs chip (left) and the microscope images, showing the growth of the hippocampal neuronal network on the chip surface (right). Reprinted with permission from (Gao et al. 2019). **(D)** Photograph of the high-density complementary metal-oxide-semiconductor technology (CMOS)-MEAs system along with the electrode array and image of a hippocampal neuronal network. Reprinted with permission from (Nieus et al., 2018). **(E)** Wire-bonded CMOS-MEAs on printed circuit board (left) and scanning electron microscopy (SEM) image of one active area, including four different electrode sizes. Reprinted with permission from (Miccoli et al., 2019).

Park et al. built humanized BBB and compared it with normoxic conditions to investigate the enhancement effect of hypoxia. To measure TEER values, they evaluated barrier functions using TEER chips generated for OoC platforms and reported enhanced barrier function in pericytes and ASTs (Henry et al., 2017; Park et al., 2019b).

4.2. Sensing neuronal activity

The BBB regulates the motion of cells, molecules, and ions between blood and neural tissues, preventing the influx of pathogens and neurotoxicants (Pulido et al., 2020). Its unique selectivity has thwarted many drug candidates at the screening phase and remains a challenge in modern medicine (Bang et al., 2019). Increased BBB permeability and subsequent leakage of non-specific molecules are strongly associated with damage caused by trauma-like neurological conditions (Takata et al., 2021). The barrier permeability may be affected by neuronal activity, which plays a pivotal role in the myelination of axons, calcium signaling and the vital functions of neurons and glial cells (e.g., survival, proliferation). Hence, undefined electrical or chemical signals transferred through sensory neurons may cause neurodegenerative diseases (e.g., AD). BBB-on-a-chip is a suitable platform for super-resolution microscopy that promotes cell co-culture accomplished with fluid flow. For instance, stimulated emission depletion-driven microfluidic assay integrated with omics leads to high-throughput outcomes in single-cell manipulation (Booth and Kim, 2012; Oddo et al., 2019). Therefore, besides BBB, one of the recent advancements in BoC systems is the real-time measurement of electrical activity. BoC platforms allow spatial and temporal resolution control of the extracellular environment and support high-resolution analysis of subcellular signals. Meanwhile, thin transparent substrates indicate automation and super-resolution imaging for precise monitoring changes correlated to cellular dynamics. These microfluidic systems can easily integrate with other sensing tools for biomarker detection, real-time electrical measurements, monitoring of cell cultures and other applications (Esch et al., 2015; Oddo et al., 2019; Whitesides, 2006).

There have numerous efforts to record the electrical activity of neuronal populations in real-time (Gao et al., 2020; Niaraki et al., 2022; Seymour et al., 2017). To this end, integrating passive and active high-density MEAs into microfluidic-based BoC platforms could provide a facile tool for understanding neural circuits and interactions (Forro et al., 2021) (Table 2). Notably, the assembly of planar/3D MEAs with transparent PDMS-based microfluidic platforms provides a controlled growth pattern, recording activity-dependent dynamics of cells (Gladkov et al., 2017; Moutaux et al., 2018; Shen et al., 2019). Moreover, prepared PDMS channels could be mounted with MEAs (Gao et al., 2021) or divided into separate modular networks connected with micro-tunnels, enabling synchronous electrical activity in a closed chain configuration (van de Wijdeven et al., 2019). Analysis of NSCs rosettes shows multiple cytokines signaling by cell-cell interaction microchip for simultaneously tracking ten cytokines (PDGF-AA, IGF-1, BDNF, GDNF, FGF-2, BMP-4, IL-6, β-NGF, CNTF, and NT-3), morphological changes and biomarkers expression. These microchips could be used in tissue

Table 2
Summary of 2D and 3D neural cell cultures monitored by passive and active MEAs (For MEA classification, studies using CMOS were listed as active and those not used as passive).

MEAs type		Device			Refs.
Active (w/ CMOS)	Passive	Purpose	Cell type	Culture period (Days *in vitro*; DIV)	
	+	Recording the spiking activity of the neurons	Primary dissociated hippocampal neurons	25	(Gladkov et al., 2017)
	+	Analyzing the effect of phencyclidine on the electrical behavior of all three brain regions	Primary harvested neuronal and glial cells	20	(Dauth et al., 2017)
	+	Development of MEMS-based 3D cell culture system for recording neuro-electrophysiological activity	SH-SY5Y and hiPSC-derived cortical neurons	21	(Bastiaens et al., 2018)
	+	Investigating the activity-dependent dynamics in the physiological context of brain circuits	Primary dissociated cortical neurons	14	(Moutaux et al., 2018)
	+	Monitoring neural network activity and intra-/inter nodal connectivity	Primary cortical neurons and ASTs	27	(van de Wijdeven et al., 2019)
	+	Recording the electrophysiological response of neuronal networks	Primary hippocampus neurons	28	(Shen et al., 2019)
	+	Multisite and dynamic monitoring of long-term bioelectrical activity changes in neurodegenerative networks	Primary dissociated hippocampal neurons	13 *Treated with Aβ oligomers for several timelines at DIV 13.	(Gao et al. 2019)
	+	Noninvasive way to monitor and support neural growth in a 3D ECM-collagen gel	hiPSC-derived neurons and ASTs	45 *Representative data were provided for DIV 38.	(Soscia et al., 2020)
	+	Monitoring the spontaneous neuronal network activities	hPSC-derived neurons	130 *32 days for pre-differentiation	(Pelkonen et al., 2020)
	+	Monitoring the neural spikes and local field potentials.	Embryo neural stem cells	10	(Gao et al., 2020)
	+	Detecting the olfactory stimuli patterns	Primary harvested olfactory receptor and bulb neurons	14	(Gao et al., 2021)
	+	Stimulation of presynaptic axons and recording the post-synaptic muscle activity	hiPSCs-derived motor neurons and myoblasts	24	(Duc et al., 2021)
	+	Interpretation of neural network dynamics in a label-free manner	hiPSCs-derived cortical neurons	79	(Demircan Yalcin et al., 2021)
	+	Real-time investigation of neurotoxicity of Aβ on neural networks	Dissociated NSCs	8 *5 days of culture and Aβ treatment for 24, 48, and 72 h	(Liu et al., 2022)
	+	Monitoring real-time cellular adhesion upon exposure to stress factors	Dopaminergic neural cells	4 * Cell network reaches the confluent state at DIV 4	(Niaraki et al., 2022)
+		Long-term electrical monitoring of changes at the cellular level regarding neurodegenerative network activity	Primary dissociated hippocampal neurons	24 * Aβ exposure at different concentrations for several timelines at DIV 24	(Amin et al., 2017)
+		Quantification of state dependency in cell culture responses	Primary dissociated hippocampal neurons	24	(Nieus et al., 2018)
+		Simultaneous monitoring of electrophysiological activity and assessment of primary neurons growth	Primary dissociated hippocampal neurons	43	(Miccoli et al., 2019)
+		Investigating the influence of electrode size-dependent parameters on neural signals	Primary dissociated cortical cells; brain slices; organotypic slice cultures	18	(Viswam et al., 2019)
+		Synaptic connectivity mapping through an intracellular neuro-electronic interface	Primary dissociated neuronal cells	33 *Data were given for intracellular experiments: DIV10-14, Extracellular: 26-33	(Abbott et al., 2020)
+		Characterization and comparison of network bursting in human motor and dopaminergic neurons	hiPSC-derived neuronal cell lines and primary dissociated neurons	42	(Ronchi et al., 2021)

architecture studies, cell morphology evaluation, analysis of cytokine signaling, and biomarker expression.

A key function of this new device is to characterize the rosette cytokine signature and analyze changes in cytokine signaling of disrupted rosette structures in cells. Other functions include modeling neurodegeneration or neuroplasticity and opioid drug reactions; analysis of genetic mutation screening and microscopy in neurodegeneration; and subset interactions using partially dissecting rosettes (Abdullah et al., 2020).

Track-Etched magnetic NanoPOre provides a framework for nanofluidic immunomagnetics to examine multiple sub-populations of brain-derived extracellular vesicles (EVs) and miRNA biomarkers isolation to develop potential detection for TBI. TENPO approaches accelerate the isolation of EVs from half a day to less than an hour, which shows the translation of this technology into a PoC device by miniaturized miRNA detection. However, detection sensitivity challenges have emerged due to the low concentration of biomarker circulation, proteolytic degradation, clearance by the kidney or liver, and the possibility of binding biomarkers to carrier proteins. Isolation of EVs biomarkers faces multiple challenges, such as the nanoscale size of EVs, isolation with a relatively long timespan (>6 h), co-purification with cellular debris, and non-selective isolate. Sorting and detecting by microfluidics into complex media can be more appropriate than nanoscale, but EVs are limited to low throughput and susceptible to nanofluid obstruction (Ko et al., 2018). An LED-mediated framework has been coupled to a microfluidic platform capable of high throughput ELISA sample detection. The platform offers superior features compared to that of conventional ELISA, such as automation, reagent volumes reduced to 200 nL, a significant decline in process time, and detection of emitted fluorescent signals that advances the relatively accurate and rapid molecular sensing of AD. Moreover, it uses the detection of a wide spectrum of Aβ peptides supported by sample fractionation with a magnetic

beads-based capillary (Mai et al., 2018). Most electrochemical sensors for detecting Aβ oxidation signals suffer from a low signal rate, especially on electrode surfaces with non-specific absorption of serum protein. magneto-immunocapture followed by fluorescent labeling was reported for sensitive determination of Aβ peptides enrichment. This strategy removes extra fluorescent dyes (Mai et al., 2015).

Physiologically relevant models for human neuromuscular junctions (Duc et al., 2021), epileptic seizures (Pelkonen et al., 2020), schizophrenia-like states (Dauth et al., 2017), AD developments, and aberrant neuronal activity (Fig. 6C) (Gao et al. 2019; Liu et al., 2022) and several others have shown the relevance of such systems for electrophysiological measurements of neuronal cells. Besides 2D neural interactions, 3D neuronal cell cultures providing more realistic data regarding neuronal network activity and drug toxicity screening have been reported for passive and active MEAs (Bastiaens et al., 2018; Demircan Yalcin et al., 2021; Shin et al., 2021; Soscia et al., 2020). Although passive MEAs (having 60–256 electrodes) have been primarily proposed in the literature, the key advantages of MEAs, using CMOS are their high resolution, identifying the activities of each neuronal cell, detecting small signals, and acquiring readouts at network cell and subcellular levels (Miccoli et al., 2019; Nieus et al., 2018; Viswam et al., 2019) (Fig. 6D–E). As such, CMOS-activated electrode arrays exploiting large-scale neuronal recordings (up to 60 thousand electrodes) (Forro et al., 2021) were reported to perform high spatiotemporal bioelectrical imaging (Amin et al., 2017), receive intracellular recordings from thousands of connected neurons (Abbott et al., 2020; Nieus et al., 2018), investigate network bursting in human motor and dopaminergic neurons, and detect cell type-specific oscillatory patterns through HD-MEAs (Ronchi et al., 2021). Furthermore, MEAs and multi-electrode array--based microfluidic chips as potential platforms offer significant benefit due to the division of neurons in specific compartments, and accurate patterns based on position cells can be high for detecting neuronal firing that probes in monoculture (Holloway et al., 2021).

4.3. Sensing neuronal metabolites

Neuronal cells express a wide range of metabolites to maintain homeostasis and respond to specific pathological states. These metabolites include potassium and calcium ions (Roberts et al., 2018), cytokines regulating cell functions during immune responses (Cakmak et al., 2022), and TNF-α, a pro-inflammatory cytokine seen in neuroinflammation that reaches elevated levels in neurodegenerative diseases (Neniskyte et al., 2014). Located at the presynaptic terminal in neurons, α-syn can indicate aggregates implicating PD (Lee et al., 2020). Highly selective and highly sensitive analyses of these metabolites in real time are important to understanding metabolic activity changes in the activities of neuronal cells. A recent study reported combining calcium sensor imaging and extracellular recordings of local field potentials of a cerebral cortex-ganglionic eminence organoid to identify neural oscillations (Samarasinghe et al., 2021). Another study investigated the use of nanoparticles of FI3, a fluoroionophore with aza-crown-ether-based sensing unit producing electromagnetic spectrum emissions ranging from green to near-infrared; the FI3 nanoparticles were efficient for real-time screening of intra- and extracellular potassium ions in neurospheroids (Mueller et al., 2018). An electrochemical sensor based on α-syn peptide-imprinted poly(EDOT-co-EDOT-OH)s detected neuronal protein α-syn accumulation in midbrain organoid culture medium generated from iPSCs of PD patients, where the sensing range was 0.065 pM–65 nM (Lee et al., 2020). More studies on integrating sensors are required for faster diffusion and clinical translation of BoC platforms.

5. Challenges and limitations of biosensor integrated BoC platforms in translation to the clinic

BoC platforms have rapidly replaced time-consuming animal studies, require trained professionals and advanced facilities, and face ethical constraints. Challenges in BoC systems accompany engineered platforms for biomimicry of the neural circuitry and 3D BBB or natural miniature tissues grown inside the microfluidic chip. Nevertheless, new flexible chips can be adaped to tissues with 3D geometry and high spatial resolution and are highly controlled customizable sensors for interfacing spheroids of various sizes, allowing following signal propagation in 3D (Kalmykov et al., 2019; Pitsalidis et al., 2018). That neurodegenerative diseases such as PD and AD are not observed in other animal species is a driver for using brain-mimic integrated platforms to comprehend the mechanisms underlying complex functions of diseases or to test newly synthesized drugs on human-like systems.

One of the most promising features of these BoC integrated biosensor systems is their ability to adapt to personalized medicine. BoC, along with microfluidic biosensors, can monitor cerebral concentrations of neurotransmitters, biomarkers and metabolic variations and allows optical analysis of interconnected cells and receptors (Weisenburger and Vaziri, 2018). As an integrated platform, BoC provides automatized screening of a vast number of analytes and creates a stable environment for efficient solubility and permeability of gas molecules, which is important to O_2 and CO_2 exchange in living cells (Liang and Yoon, 2021). Although these systems promote the study of neural cells and circuitry in a dimensionally and temporally controlled environment, biological and technical challenges must be considered. One biological challenge in BoC design is that the brain is soft, rough, and has an odd shape. The constant rhythmic motion of the brain can disrupt real-time monitoring (Choi et al., 2021). Spatial cell arrangements, biocompatibility, and mechanical stability under physiological conditions are challenging parameters (Li and Tian, 2018). Scale must be considered in miniaturizing a device mimicking brain behavior (Amirifar et al., 2022). Co-culture of different neural cell types to form the brain and cell density is the other biological challenge to be considered. To prevent optical challenges, the microchannels of the microfluidic biosensor must be built of transparent layers, which permits imaging under microscopy and high-resolution analysis in normal and pathophysiological conditions. Advanced natural and synthetic hybrid polymers might be a solution to these problems as a building materials.

The minor variations within the building material, especially for large-scale production and fabrication processes, could also affect cell viability, another technical consideration in 3D microfluidic BoC systems. Because of their electroactive MEAs and fluidic channels, these systems are limited to monitorization of different microenvironmental factors (Mofazzal Jahromi et al., 2019). Soft-lithography is one of the most common approaches to consistent production of BoC. However, the need for masks, low bio-resistance, and a sophisticated infrastructure could limit its applicability (Puryear et al., 2020). Soft-lithography could replace robust production methods like 3D printing to address this limitation. 3D printing enables proof-of-concept studies to large-scale clinical trials by integrating different elements with various mechanical behaviors into the same device. A 3D printed microfluidic analyzer connected to an electrochemical biosensor for screening dynamic variations in lactate, glutamate, and glucose in injured brain patients has been designed in a microdialysate stream at μL/min flow rate (Samper et al., 2019); 3D printing was realized with an expensive Ultra 3SP machine, and pre and post-operational steps were labor-intensive. Still, results are promising for clinical translation. 3D printing provides accurate and large-scale mass production, but inadequate optical transparency prevents high-resolution imaging (Leung et al., 2022) and the bioincompatibility of 3D printed resins remains to be solved.

Optical approaches to analysis of neural activity have been proposed as an alternative to electrochemical-based BoC. These optical systems are less invasive than their electrochemical counterparts and do not need close proximity to target cells, but photo-bleaching and complex instrumentation limit their applicability. To overcome these limitations, an electrochemical and optical system integrated inside an incubator was developed (Shin et al., 2021). A board was utilized to record electrophysiological activity using 63 Pt-black microelectrodes distributed

over 18 vertical shanks in a PDMS microfluidic chip. For optical stimulation, a small LED was incorporated into the chip. This eliminates external light sources and reduces production costs but requires several optical interfaces, which is labor-intensive, and uses Pt electrodes, which create an interfacial resistance that can cause signal instability. Despite these concerns, the design is promising for adapting CMOS-based MEAs for biosensing applications. With technological advances, integrating a light source array onto the tip of every shank would permit more complex circuits *in vitro*, which could open doors for real-time monitoring in clinical applications.

The surrounding aqueous droplet compartment of the liquid-liquid interface presents a significant challenge but this can be stabilized using surfactants. Therefore, droplet coalescence should occur when necessary. Meanwhile, different stabilization methods are needed for droplet storage according to experimental requirements, such as neurological factors (Kaminski and Garstecki, 2017; Zhou et al., 2021).

A critical challenge to be addressed is protein aggregation assays using standard bulky methods by multi-well plates over extended time periods, such as mass-spectrometry and protein purification techniques based on chromatographic or gel line analysis techniques. To solve such problems, the microfluidic channels can potentially perform high throughput screens as a favorably alternative to identification of amyloid formation inhibitors (Ciryam et al., 2013; Guo et al., 2012; Herling et al., 2018; Taly et al., 2007).

The separation and detection of monomeric Aβ peptides with their trace quantities (0.1–10 nM) in CSF are very challenging due to (i) their tendency to self-assemble and aggregate in the form of heterogeneous mixtures; (ii) binding to other molecular partners; (iii) dedicating microfluidic devices as it is not possible to analysis with μL-plate-mediated sub μL droplets. So far, efforts have addressed improving the detection of Aβ peptides microfluidic droplets in the early stages of AD (Kim et al., 2015; Mai et al., 2018).

Microfluidic-based fluorescent signal measurement requires the fluorescence microscope (FM) and atomic force microscope (AFM) for monitoring micro-cantilever deflection and displacement or the resonant frequency of the micro-electro-mechanical systems cantilever sensor. Both microscopes must be miniaturized before they can be applied to PoC (Song et al., 2020).

Detection of neurotransmitters for analysis is limited because of high complexity. Fractionation-based processes such as liquid chromatography, capillary electrophoresis, spin columns, and packed pipette tips reduce this complexity. Meanwhile, combining sample cleanup and on-chip analyte detection can reduce the time spent on sample cleanup (Croushore and Sweedler, 2013).

The opacity of 3D MEAs makes simultaneous optical imaging difficult and hinders cell visibility. Optically transparent indium tin oxide electrodes allow imaging, but their resistance and signal-to-noise performance are inferior to those of opaque (Forro et al., 2021). To solve this problem, TiNi-coated electrodes have been produced with no loss of transparency using atomic layer deposition (Ryynänen et al., 2019). Ag/AgCl, Pt, Pt black, Au, Ti, and metal electrodes have also been used in cell studies, while metals such as Co and Ag have shown toxic effects on cultured cells. Modified electrodes with large surface area, lower impedance, and transparency for optical imaging can be used for integrated BoC with biosensors (Fuchs et al., 2021). Due to their complexity, BoC-integrated platforms present challenges that remain to be addressed. For understanding the underlying mechanisms of brain-related diseases, the development of an integrated platform that combines organ models, microfluidic components, and biosensors is open to improvement.

In conclusion, BoC translation into the clinic requires more time to monitor the brain's electrophysiological activity and such parameters as metabolites and biomarkers. In literature, different methods have been introduced to detect biological molecules, and physical, electrochemical, biochemical, and optical sensing platforms can be integrated for *in situ* automated microenvironment analysis. Despite significant technological advances, translation of these findings to the clinical setting and the treatment of patients with neurological disorders has been slower than expected. Furthermore, standardization and regulatory endorsement challenges must be confronted in the next few years. Promising proof-of-concept studies should not stay in the "valley of death," the gap between bench research and clinical applications (Seyhan, 2019). Multidisciplinary approaches and close collaboration between clinicians, health experts, engineers, and biomedical researchers are critical for developing new technologies that can be successfully translated into clinical settings.

6. Conclusion and future outlook

BoC platforms are preclinical tools with the potential to significantly reduce, refine, and even replace animal experiments in drug development. One of the significant virtues of microfluidic BBB platforms is their ability to monitor and record biological reactions to a variety of stimuli at once. In this respect, BoC platforms permit faster development of new compounds, lower the cost of reagents and cells and eliminate growing ethical concerns about animal testing by using cells of human origin that are more predictive of human-specific clinical effects (Arora et al., 2011; Jin et al., 2020; Ma et al., 2021). Electrochemical and optical biosensors are now the favored option for real-time observation of biological activities. However, they have substantial limitations, including poor resolution and short sensor lifetime due to electrode saturation (Li and Lee, 2020; Zhu et al., 2021).

Interface complexity should be eliminated to the greatest extent feasible to build BoC platforms so that it will be eventually compatible with standardized forms typically used by biotech and pharmaceutical businesses. Collaborations with diverse disciplines must create sensors capable of automated assessment of BoC systems in continuous, real-time, and high-throughput (Gonçalves et al., 2022; Mir et al., 2022). Once these hurdles have been cleared, BoC, including next-generation biosensors, will enable accurate, detailed simulation of complicated and specialized pathologic situations. BoC, for example, might be immensely useful in tumor research; studying and monitoring the interactions of tumor tissues with other tissues will advance drug detection, biomarker recognition, and long-term pharmaceutical use and improve cancer treatment (Petrovszki et al. 2022, 2022zsoylu et al., 2022). Because of this, multi-sensor and multi-organ platforms will be significant for testing drugs for cancer and other diseases, and will eventually replace animal models. Because BoC allows for the simulation of organ–organ interactions using human-derived cells, difficulties associated with phases in clinical stages and subsequent medication withdrawal may significantly decrease (Wang et al., 2005). Microfluidic BoC systems can potentially push the boundaries of detection devices to assay nervous cells' intracellular and extracellular media. This can be an appropriate alternative to use of conventional animal models for disease monitoring. The US Food and Drug Administration proposed using microfluidic-mediated technologies for experiments prior to animal model testing and subsequent human clinical trials (Mofazzal Jahromi et al., 2019). It is to be expected that BoC combining numerous biosensors will be commonly used in future laboratory research, clinical applications, and personalized medicine studies.

Author contribution

Berivan Cecen: Conceptualization, Validation, Formal analysis, Investigation, Writing original draft preparation, Review & editing. **Ecem Saygili:** Investigation, Visualization, Writing- Original draft preparation. **Iman Zare:** Investigation, Visualization, Writing- Original draft preparation. **Omid Nejati:** Investigation, Visualization, Writing- Original draft preparation. **Danial Khorsandi:** Investigation, Visualization, Writing- Original draft preparation. **Atefeh Zarepour:** Investigation, Visualization, Writing- Original draft preparation. **Emine Alarcin:** Investigation, Visualization, Writing- Original draft

preparation.

Ali Zarrabi: Investigation, Visualization, Validation, Writing- Original draft preparation. **Seda Nur Topkaya:** Investigation, Writing-Original draft preparation. **Ozlem Yesil-Celiktas:** Conceptualization, Methodology, Validation, Investigation, Data curation, Formal analysis, Project administration, Supervision, Visualization, Writing – review & editing. **Ebrahim Mostafavi:** Conceptualization, Methodology, Validation, Investigation, Data curation, Formal analysis, Project administration, Supervision, Visualization, Writing – review & editing. **Ayça Bal Öztürk:** Conceptualization, Methodology, Validation, Investigation, Data curation, Formal analysis, Project administration, Supervision, Visualization, Writing – review & editing.

Declaration of competing interest

The authors declare that they have no known competing financial interests or personal relationships that could have appeared to influence the work reported in this paper.

Data availability

No data was used for the research described in the article.

Acknowledgements

A.B.O acknowledges the support from the Scientific and Technological Research Council of Turkey (TUBITAK) (221M724). E.M. would like to acknowledge the support from the National Institute of Biomedical Imaging and Bioengineering (5T32EB009035). O.Y.C. acknowledges the support from the Research Fund of Ege University, International Research Cooperation Project under grant number FUA-2020-22187.

References

Aazmi, A., Zhou, H., Lv, W., Yu, M., Xu, X., Yang, H., Zhang, Y.S., Ma, L., 2022. iScience, 104110.
Abbott, J., Ye, T., Krenek, K., Gertner, R.S., Ban, S., Kim, Y., Qin, L., Wu, W., Park, H., Ham, D., 2020. Nat Biomed Eng 4 (2), 232–241.
Abdullah, M.A., Amini, N., Yang, L., Paluh, J.L., Wang, J., 2020. Lab Chip 20 (21), 3980–3995.
Aday, S., Cecchelli, R., Hallier-Vanuxeem, D., Dehouck, M.P., Ferreira, L., 2016. Trends Biotechnol. 34 (5), 382–393.
Adegbola, A., Bury, L.A., Fu, C., Zhang, M., Wynshaw-Boris, A., 2017. Stem Cells Translational Medicine 6 (12), 2062–2070.
Adriani, G., Ma, D., Pavesi, A., Kamm, R.D., Goh, E.L., 2017. Lab Chip 17 (3), 448–459.
Agostini, M., Amato, F., Vieri, M., Greco, G., Tonazzini, I., Baroncelli, L., Caleo, M., Vannini, E., Santi, M., Signore, G.J.B., 2021. Bioelectronics 172, 112774.
Ahadian, S., Civitarese, R., Bannerman, D., Mohammadi, M.H., Lu, R., Wang, E., Davenport-Huyer, L., Lai, B., Zhang, B., Zhao, Y., 2018. Advanced Healthcare Materials 7 (2), 1700506.
Ahn, S.I., Sei, Y.J., Park, H.J., Kim, J., Ryu, Y., Choi, J.J., Sung, H.J., MacDonald, T.J., Levey, A.I., Kim, Y., 2020. Nat. Commun. 11 (1), 175.
Akhtar, A., Andleeb, A., Waris, T.S., Bazzar, M., Moradi, A.R., Awan, N.R., Yar, M., 2021. J. Contr. Release 330, 1152–1167.
Aleman, J., Kilic, T., Mille, L.S., Shin, S.R., Zhang, Y.S., 2021. Nat. Protoc. 16 (5), 2564–2593.
Alvarez, C.V., Garcia-Lavandeira, M., Garcia-Rendueles, M.E., Diaz-Rodriguez, E., Garcia-Rendueles, A.R., Perez-Romero, S., Vila, T.V., Rodrigues, J.S., Lear, P.V., Bravo, S.B., 2012. J. Mol. Endocrinol. 49 (2), R89–R111.
Ameri, M., Shabaninejad, Z., Movahedpour, A., Sahebkar, A., Mohammadi, S., Hosseindoost, S., Ebrahimi, M.S., Savardashtaki, A., Karimipour, M., Mirzaei, 2020. Int. J. Biol. Macromol. 162, 1100–1108.
Amin, H., Nieus, T., Lonardoni, D., Maccione, A., Berdondini, L., 2017. Sci. Rep. 7 (1), 2460.
Amirifar, L., Shamloo, A., Nasiri, R., de Barros, N.R., Wang, Z.Z., Unluturk, B.D., Libanori, A., Ievglevskyi, O., Diltemiz, S.E., Sances, S., 2022. Biomaterials 285, 121531.
Ammar, M., Smadja, C., Phuong, L.G.T., Azzouz, M., Vigneron, J., Etcheberry, A., Taverna, M., Dufour-Gergam, E., 2013. Biosens. Bioelectron. 40 (1), 329–335.
Ansari, A.A., Malhotra, B.D., 2022. Coord. Chem. Rev. 452, 214282.
Arandian, A., Bagheri, Z., Ehtesabi, H., Najafi Nobar, S., Aminoroaya, N., Samimi, A., Latifi, H., 2019. Small 15 (28), 1900737.
Arora, T., Mehta, A., Joshi, V., Mehta, K., Rathor, N., Mediratta, P., Sharma, K., 2011. Indian J. Pharmaceut. Sci. 73 (1), 1.
Azimzadeh, M., Khashayar, P., Amereh, M., Tasnim, N., Hoorfar, M., Akbari, M., 2021. Biosensors 12 (1), 6.
Azizgolshani, H., Coppeta, J., Vedula, E., Marr, E., Cain, B., Luu, R., Lech, M., Kann, S., Mulhern, T., Tandon, V., 2021. Lab Chip 21 (8), 1454–1474.
Banerjee, A., Arha, M., Choudhary, S., Ashton, R.S., Bhatia, S.R., Schaffer, D.V., Kane, R. S., 2009. Biomaterials 30 (27), 4695–4699.
Bang, S., Lee, S.R., Ko, J., Son, K., Tahk, D., Ahn, J., Im, C., Jeon, N.L., 2017. Sci. Rep. 7 (1), 1–10.
Bang, S., Jeong, S., Choi, N., Kim, H.N., 2019. Biomicrofluidics 13 (5), 051301.
Bang, S., Lee, S., Choi, N., Kim, H.N., 2021. Advanced Healthcare Materials 10 (12), 2002119.
Bastiaens, A.J., Frimat, J.P., van Nunen, T., Schurink, B., Homburg, E.F.G.A., Luttge, R., 2018. Front. Mech. Eng. 4, 21.
Bates, G.P., Dorsey, R., Gusella, J.F., Hayden, M.R., Kay, C., Leavitt, B.R., Nance, M., Ross, C.A., Scahill, R.I., Wetzel, R., 2015. Nature Reviews 1 (1), 1–21.
Bednarek, R.J.M., 2022. Methods and Protocols 5 (1), 17.
Bhattacharjee, N., Folch, A., 2017. Microsystems & Nanoengineering 3 (1), 1–14.
Blanco-López, M., Lobo-Castañón, M., Miranda-Ordieres, A., Tunon-Blanco, P., 2004. TrAC, Trends Anal. Chem. 23 (1), 36–48.
Booth, R., Kim, H., 2012. Lab Chip 12 (10), 1784–1792.
Brazaca, L.C., Sampaio, I., Zucolotto, V., Janegitz, B.C.J.T., 2020. Talanta 210, 120644.
Brofiga, M., Pisano, M., Raiteri, R., Massobrio, P., 2021. J. Neural. 18, 041005.
Brofiga, M., Pisano, M., Tedesco, M., Boccaccio, A., Massobrio, P., 2022. Cerebr. Cortex 32 (9), 1866–1881.
Butt, H.J., 1996. J. Colloid Interface Sci. 180 (1), 251–260.
Caballero, D., Kaushik, S., Correlo, V., Oliveira, J.M., Reis, R., Kundu, S., 2017. Biomaterials 149, 98–115.
Cakmak, B., Saglam-Metiner, P., Beceren, G., Zhang, Y.S., Yesil-Celiktas, O., 2022. Bio-Design and Manufacturing 1–16.
Carter, S.-S.D., Atif, A.R., Kadekar, S., Lanekoff, I., Engqvist, H., Varghese, O.P., Tenje, M., Mestres, G., 2020. Organs-on-a-Chip 2, 100004.
Cavaliere, F., Cerf, L., Dehay, B., Ramos-Gonzalez, P., De Giorgi, F., Bourdenx, M., Bessede, A., Obeso, J.A., Matute, C., Ichas, F., 2017. Neurobiol. Dis. 103, 101–112.
Chadha, U., Bhardwaj, P., Agarwal, R., Rawat, P., Agarwal, R., Gupta, I., Panjwani, M., Singh, S., Ahuja, C., Selvaraj, S.K., 2022. J. Ind. Eng. 109, 21–51.
Chanda, K., Balamurali, M., 2021. Chem. Soc. Rev. 50 (6), 3706–3719.
Chen, G.Y., Thundat, T., Wachter, E., Warmack, R., 1995. J. Appl. Phys. 77 (8), 3618–3622.
Chen, J.S., Chen, P.-F., Lin, H.T.H., Huang, N.T., 2020. Analyst 145 (23), 7654–7661.
Cho, H., Hashimoto, T., Wong, E., Hori, Y., Wood, L.B., Zhao, L., Haigis, K.M., Hyman, B. T., Irimia, D., 2013. Sci. Rep. 3 (1), 1–7.
Choi, J.S., Lee, H.J., Rajaraman, S., Kim, D.H., 2021. Biosens. Bioelectron. 171, 112687.
Chwalek, K., Tang-Schomer, M.D., Omenetto, F.G., Kaplan, D.L., 2015. Nat. Protoc. 10 (9), 1362–1373.
Ciryam, P., Tartaglia, G.G., Morimoto, R.I., Dobson, C.M., Vendruscolo, M., 2013. Cell Rep. 5 (3), 781–790.
Croushore, C.A., Sweedler, J.V., 2013. Lab Chip 13 (9), 1666–1676.
Curto, V.F., Marchiori, B., Hama, A., Pappa, A.M., Ferro, M.P., Braendlein, M., Rivnay, J., Fiocchi, M., Malliaras, G.G., Ramuz, M., Owens, R.M., 2017. Microsystems & Nanoengineering 3 (1), 17028.
Damborský, P., Švitel, J., Katrlík, J., 2016. Essays Biochem. 60 (1), 91–100.
Dauth, S., Maoz, B.M., Sheehy, S.P., Hemphill, M.A., Murty, T., Macedonia, M.K., Greer, A.M., Budnik, B., Parker, K.K., 2017. J. Neurophysiol. 117 (3), 1320–1341.
De Filippis, L., Zalfa, C., Ferrari, D., 2017. CNS Neurol. Disord. - Drug Targets 16 (8), 915–926.
de Oliveira, T.R., Erbereli, C.R., Manzine, P.R., Magalhaes, T.N., Balthazar, M.L., Cominetti, M.R., Faria, R.C., 2020a. ACS Sens. 5 (4), 1010–1019.
de Oliveira, T.R., Erbereli, C.R., Manzine, P.R., Magalhães, T.N.C., Balthazar, M.L.F., Cominetti, M.R., Faria, R.C., 2020b. ACS Sens. 5 (4), 1010–1019.
De Vitis, E., La Pesa, V., Gervaso, F., Romano, A., Quattrini, A., Gigli, G., Moroni, L., Polini, A., 2021. Sci. Rep. 11 (1), 1–12.
Deleglise, B., Magnifico, S., Duplus, E., Vaur, P., Soubeyre, V., Belle, M., Vignes, M., Viovy, J.L., Jacotot, E., Peyrin, J.M., 2014. Acta Neuropathologica Communications 2 (1), 1–9.
Demircan Yalcin, Y., Bastiaens, A.J., Frimat, J.P., Luttge, R., 2021. J. Vac. Sci. Technol. B 39 (6), 064004.
Dilgin, Y., Karakaya, S., Dilgin, D.G., 2021. Quantum Dots-Based Photoelectrochemical Sensors and Biosensors. Electroanalytical Applications of Quantum Dot-Based Biosensors. Elsevier, pp. 209–269.
Dostálek, J., Vaisocherová, H., Homola, J., 2005. Sensor. Actuator. B Chem. 108 (1–2), 758–764.
Duc, P., Vignes, M., Hugon, G., Sebban, A., Carnac, G., Malyshev, E., Charlot, B., Rage, F., 2021. Lab Chip 21 (21), 4223–4236.
Eiraku, M., Takata, N., Ishibashi, H., Kawada, M., Sakakura, E., Okuda, S., Sekiguchi, K., Adachi, T., Sasai, Y., 2011. Nature 472 (7341), 51–56.
Engler, A.J., Sen, S., Sweeney, H.L., Discher, D.E., 2006. Cell 126 (4), 677–689.
Eom, K., Park, H.S., Yoon, D.S., Kwon, T., 2011. Phys. Rep. 503 (4–5), 115–163.
Esch, E.W., Bahinski, A., Huh, D., 2015. Nat. Rev. Drug Discov. 14 (4), 248–260.
Fan, Y., Nguyen, D.T., Akay, Y., Xu, F., Akay, M., 2016. Sci. Rep. 6 (1), 1–12.
Fantuzzo, J.A., De Filippis, L., McGowan, H., Yang, N., Ng, Y.H., Halikere, A., Liu, J.-J., Hart, R.P., Wernig, M., Zahn, J.D., 2017. Technology 5, 87–97, 02.
Ferrari, E., Palma, C., Vesentini, S., Occhetta, P., Rasponi, M., 2020. Biosensors 10 (9), 110.
Flanagan, L.A., Ju, Y.-E., Marg, B., Osterfield, M., Janmey, P.A., 2002. Neuroreport 13 (18), 2411.

Forro, C., Caron, D., Angotzi, G.N., Gallo, V., Berdondini, L., Santoro, F., Palazzolo, G., Panuccio, G., 2021. Micromachines 12 (2).
Fuchs, S., Johansson, S., Tjell, A.Ø., Werr, G., Mayr, T., Tenje, M., 2021. ACS Biomater. Sci. Eng. 7 (7), 2926–2948.
Gagni, P., Sola, L., Cretich, M., Chiari, M., 2013. Biosens. Bioelectron. 47, 490–495.
Galan, E.A., Zhao, H., Wang, X., Dai, Q., Huck, W.T., Ma, S., 2020. Matter 3 (6), 1893–1922.
Gale, B.K., Jafek, A.R., Lambert, C.J., Goenner, B.L., Moghimifam, H., Nze, U.C., Kamarapu, S.K., 2018. Inventions 3 (3), 60.
Gao, F., Gao, K., He, C., Liu, M., Wan, H., Wang, P., 2019. Biosens. Bioelectron. 133, 183–191.
Gao, F., Luo, J., Song, Y., He, E., Zhang, Y., Xiao, G., Cai, X., 2020. Nanotechnology and Precision Engineering 3 (2), 69–74.
Gao, K., Gao, F., Li, J., He, C., Liu, M., Zhu, Q., Qian, Z., Ma, T., Wang, P., 2021. Biosens. Bioelectron. 171, 112739.
Gladkov, A., Pigareva, Y., Kutyina, D., Kolpakov, V., Bukatin, A., Mukhina, I., Kazantsev, V., Pimashkin, A., 2017. Sci. Rep. 7 (1), 15625.
Gokaltun, A., Yarmush, M.L., Asatekin, A., Usta, O.B., 2017. Technology 5, 1–12, 01.
Gonçalves, I.M., Rodrigues, R.O., Moita, A.S., Hori, T., Kaji, H., Lima, R.A., Minas, G., 2022. Bioprinting, e00202.
Grieshaber, D., MacKenzie, R., Vörös, J., Reimhult, E., 2008. Sensors 8 (3), 1400–1458.
Guo, M.T., Rotem, A., Heyman, J.A., Weitz, D.A., 2012. Lab Chip 12 (12), 2146–2155.
Haeberle, S., Zengerle, R., 2007. Lab Chip 7 (9), 1094–1110.
Harberts, J., Fendler, C., Teuber, J., Siegmund, M., Silva, A., Rieck, N., Wolpert, M., Zierold, R., Blick, R.H., 2020. ACS Nano 14 (10), 13091–13102.
He, Z., Elbaz, A., Gao, B., Zhang, J., Su, E., Gu, Z., 2018. Advanced Healthcare Materials 7 (5), 1701306.
Heller, A., Feldman, B., 2008. Chem. Rev. 108 (7), 2482–2505.
Henry, O.Y.F., Villenave, R., Cronce, M.J., Leineweber, W.D., Benz, M.A., Ingber, D.E., 2017. Lab Chip 17 (13), 2264–2271.
Herland, A., van der Meer, A.D., FitzGerald, E.A., Park, T.-E., Sleeboom, J.J.F., Ingber, D. E., 2016. PLoS One 11 (3), e0150360.
Herling, T.W., Levin, A., Saar, K.L., Dobson, C.M., Knowles, T.P.J., 2018. Lab Chip 18 (7), 999–1016.
Hoarau-Véchot, J., Rafii, A., Touboul, C., Pasquier, J., 2018. Int. J. Mol. Sci. 19 (1), 181.
Holloway, P.M., Willaime-Morawek, S., Siow, R., Barber, M., Owens, R.M., Sharma, A.D., Rowan, W., Hill, E., Zagnoni, M., 2021. J. Neurosci. Res. 99 (5), 1276–1307.
Homola, J., Vaisocherová, H., Dostálek, J., Piliarik, M., 2005. Methods 37 (1), 26–36.
Hu, R., Diao, J., Li, J., Tang, Z., Li, X., Leitz, J., Long, J., Liu, J., Yu, D., Zhao, Q., 2016. Sci. Rep. 6 (1), 1–11.
Huh, D., Matthews, B.D., Mammoto, A., Montoya-Zavala, M., Hsin, H.Y., Ingber, D.E., 2010. Science 328 (5986), 1662–1668.
Ingber, D.E., 2022. Nat. Rev. Genet. 1–25.
Jagtiani, E., Yeolekar, M., Naik, S., Patravale, V., 2022. J. Contr. Release. 343, 13–30.
Jain, A., Mathur, T., Pandian, N.K., Selahi, A., 2020. Organ-on-a-chip and 3D Printing as Preclinical Models for Medical Research and Practice. Precision Medicine for Investigators, Practitioners and Providers. Elsevier, pp. 83–95.
Janata, J., 2009. Conductometric Sensors. Principles of Chemical Sensors. Springer, pp. 241–266.
Jeong, S., Kim, S., Buonocore, J., Park, J., Welsh, C.J., Li, J., Han, A., 2018. IEEE Trans. Biomed. Eng. 65 (2), 431–439.
Jin, I.S., Yoon, M.S., Park, C.-W., Hong, J.T., Chung, Y.B., Kim, J.S., Shin, D.H., 2020. Journal of Pharmaceutical Investigation 50 (3), 327–335.
Jo, J., Xiao, Y., Sun, A.X., Cukuroglu, E., Tran, H.D., Göke, J., Tan, Z.Y., Saw, T.Y., Tan, C.P., Lokman, H., 2016. Cell Stem Cell 19 (2), 248–257.
Kalmykov, A., Huang, C., Bliley, J., Shiwarski, D., Tashman, J., Abdullah, A., Rastogi, S. K., Shukla, S., Mataev, E., Feinberg, A.W., 2019. Sci. Adv. 5 (8), eaax0729.
Kaminski, T.S., Garstecki, P., 2017. Chem. Soc. Rev. 46 (20), 6210–6226.
Kane, K.I.W., Moreno, E.L., Hachi, S., Walter, M., Jarazo, J., Oliveira, M.A.P., Hankemeier, T., Vulto, P., Schwamborn, J.C., Thoma, M., 2019. Sci. Rep. 9 (1), 1–12.
Kang, S., Zhao, K., Yu, D.G., Zheng, X., Huang, C., 2022. Advanced Fiber Materials 1–32.
Karimi-Maleh, H., Karimi, F., Alizadeh, M., Sanati, A.L., 2020. The Chemical Reports 20 (7), 682–692.
Kavand, H., Nasiri, R., Herland, A.J.A.M., 2022. Adv. Mater. 34 (17), 2107876.
Khalid, M.A.U., Kim, Y.S., Ali, M., Lee, B.G., Cho, Y.J., Choi, K.H., 2020. Biochem. Eng. J. 155, 107469.
Khan, N.I., Song, E.J.M., 2020. Micromachines 11 (2), 220.
Khorablou, Z., Shahdost-Fard, F., Razmi, H., Yola, M.L., Karimi-Maleh, H.J.C., 2021. Chemosphere 278, 130393.
Khorsandi, D., Palacios, S., Gaslain, Y., Emsellem, C., Combalia, J., Cortés, J., Khademhosseini, A., 2019. BMJ Specialist Journals 29 (4).
Khorsandi, D., Nodehi, M., Waqar, T., Shabani, M., Kamare, B., Zare, E.N., Ersoy, S., Annabestani, M., Çelebi, M.F., Kafadenk, A., 2021. Journal of Nanomaterials 2021, 1-16.
Kilic, O., Pamies, D., Lavell, E., Schiapparelli, P., Feng, Y., Hartung, T., Bal-Price, A., Hogberg, H.T., Quinones-Hinojosa, A., Guerrero-Cazares, H., 2016. Lab Chip 16 (21), 4152–4162.
Kilic, T., Navaee, F., Stradolini, F., Renaud, P., Carrara, S., 2018. Microphysiological Systems 2, 1–32.
Kim, J.A., Kim, M., Kang, S.M., Lim, K.T., Kim, T.S., Kang, J.Y., 2015. Biosens. Bioelectron. 67, 724–732.
Kim, Y., Yoo, Y.K., Kim, H.Y., Roh, J.H., Kim, J., Baek, S., Lee, J.C., Kim, H.J., Chae, M.S., Jeong, D., 2019. Sci. Adv. 5 (4), eaav1388.
Kim, H.J., Park, D., Yun, G., Kim, H., Kim, H.G., Lee, K.M., Hong, I.K., Park, K.C., San Lee, J., Hwang, K.S., 2021. Lab Chip 21 (23), 4557–4565.
Kim, J.W., Choi, Y.Y., Park, S.H., Ha, J.H., Lee, H.U., Kang, T., Sun, W., Chung, B.G., 2022. Lab Chip 22 (11), 2122–2130.
Ko, J., Hemphill, M., Yang, Z., Sewell, E., Na, Y.J., Sandsmark, D.K., Haber, M., Fisher, S. A., Torre, E.A., Svane, K.C., Omelchenko, A., Firestein, B.L., Diaz-Arrastia, R., Kim, J., Meaney, D.F., Issadore, D., 2018. Lab Chip 18 (23), 3617–3630.
Koklu, A., Wustoni, S., Musteata, V.E., Ohayon, D., Moser, M., McCulloch, I., Nunes, S.P., Inal, S., 2021. ACS Nano 15 (5), 8130–8141.
Koo, Y., Hawkins, B.T., Yun, Y., 2018. Sci. Rep. 8 (1), 1–7.
Kratz, S.R.A., Höll, G., Schuller, P., Ertl, P., Rothbauer, M., 2019. Biosensors 9 (3), 110.
Krefft, O., Jabali, A., Iefremova, V., Koch, P., Ladewig, J., 2018. JoVE (131), e56768.
Lancaster, M.A., Renner, M., Martin, C.-A., Wenzel, D., Bicknell, L.S., Hurles, M.E., Homfray, T., Penninger, J.M., Jackson, A.P., Knoblich, J.A., 2013. Nature 501 (7467), 373–379.
Lecuyer, M.A., Kebir, H., Prat, A., 2016. Biochim. Biophys. Acta (BBA) - Mol. Basis Dis. 1862 (3), 472–482.
Lee, M.H., Liu, K.T., Thomas, J.L., Su, Z.L., O'Hare, D., van Wuellen, T., Chamarro, J.M., Bolognin, S., Luo, S.C., Schwamborn, J.C., Lin, H.Y., 2020. ACS Appl. Nano Mater. 3 (8), 8027–8036.
Leung, C.M., de Haan, P., Ronaldson-Bouchard, K., Kim, G.-A., Ko, J., Rho, H.S., Chen, Z., Habibovic, P., Jeon, N.L., Takayama, S., Shuler, M.L., Vunjak-Novakovic, G., Frey, O., Verpoorte, E., Toh, Y.C., 2022. Nature Reviews Methods Primers 2 (1), 1–29.
Li, Y.C.E., Lee, I.C., 2020. Biosensors 10 (8), 88.
Li, X., Tian, T., 2018. Anal. Methods 10 (26), 3122–3130.
Li, X., Hu, H., Zhao, S., Liu, Y.M., 2016. Anal. Chem. 88 (10), 5338–5344.
Li, Z., Li, D., Guo, Y., Wang, Y., Su, W., 2021. Biotechnol. Lett. 43 (2), 383–392.
Liang, Y., Yoon, J.Y., 2021. Sensors and Actuators Reports 3, 100031.
Liao, Z., Zhang, Y., Li, Y., Miao, Y., Gao, S., Lin, F., Deng, Y., Geng, L., 2019. Biosens. Bioelectron. 126, 697–706.
Liu, N.-C., Liang, C.-C., Li, Y.-C.E., Lee, I.C., 2022. Pharmaceutics 14 (5).
Lopes, L.C., Santos, A., Bueno, P.R.J.S., Reports, A., 2022. Sensors and Actuators Reports 4, 100087.
Lu, J.K., Ghode, P., Thakor, N.V., 2022. Handbook of Biochips 601–630.
Ma, C., Peng, Y., Li, H., Chen, W., 2021. Trends Pharmacol. Sci. 42 (2), 119–133.
Mai, T.D., Pereiro, I., Hiraoui, M., Viovy, J.-L., Descroix, S., Taverna, M., Smadja, C., 2015. Analyst 140 (17), 5891–5900.
Mai, T.D., Ferraro, D., Aboud, N., Renault, R., Serra, M., Tran, N.T., Viovy, J.-L., Smadja, C., Descroix, S., Taverna, M., 2018. Sensor. Actuator. B Chem. 255, 2126–2135.
Maoz, B.M., 2021. APL Bioengineering 5 (3), 030902.
Maoz, B.M., Herland, A., FitzGerald, E.A., Grevesse, T., Vidoudez, C., Pacheco, A.R., Sheehy, S.P., Park, T.-E., Dauth, S., Mannix, R., 2018. Nat. Biotechnol. 36 (9), 865–874.
Mark, D., Haeberle, S., Roth, G., Stetten, F.v., Zengerle, R., 2010. Microfluidics Based Microsystems 305–376.
Marrero, D., Pujol-Vila, F., Vera, D., Gabriel, G., Illa, X., Elizalde-Torrent, A., Alvarez, M., Villa, R., 2021. Biosens. Bioelectron. 181, 113156.
Matthews, C.J., Andrews, E.S., Patrick, W.M., 2021. Anal. Chim. Acta 1156, 338218.
Miccoli, B., Lopez, C.M., Goikoetxea, E., Putzeys, J., Sekeri, M., Krylychkina, O., Chang, S.W., Firrincieli, A., Andrei, A., Reumers, V., Braeken, D., 2019. Front. Neurosci. 13, 641.
Mir, M., Palma-Florez, S., Lagunas, A., López-Martínez, M.J., Samitier, J., 2022. ACS Sens 7 (5), 1237–1247.
Modena, M.M., Chawla, K., Misun, P.M., Hierlemann, A., 2018. ACS Chem. Biol. 13 (7), 1767–1784.
Mofazzal Jahromi, M.A., Abdoli, A., Rahmanian, M., Bardania, H., Bayandori, M., Moosavi Basri, S.M., Kalbasi, A., Aref, A.R., Karimi, M., Hamblin, M.R., 2019. Mol. Neurobiol. 56 (12), 8489–8512.
Mollarasouli, F., Kurbanoglu, S., Ozkan, S.A., 2019. Biosensors 9 (3), 86.
Monzel, A.S., Smits, L.M., Hemmer, K., Hachi, S., Moreno, E.L., van Wuellen, T., Jarazo, J., Walter, J., Brüggemann, I., Boussaad, I., 2017. Stem Cell Rep. 8 (5), 1144–1154.
Motallebnejad, P., Thomas, A., Swisher, S.L., Azarin, S.M., 2019. Biomicrofluidics 13 (6), 064119.
Moulin, A., O'shea, S., Welland, M.E., 2000. Ultramicroscopy 82 (1–4), 23–31.
Mousavi, M.P., Ainla, A., Tan, E.K., Abd El-Rahman, M.K., Yoshida, Y., Yuan, L., Sigurslid, H.H., Arkan, N., Yip, M.C., Abrahamsson, C.K., 2018. Lab Chip 18 (15), 2279–2290.
Mousavi Shaegh, S.A., De Ferrari, F., Zhang, Y.S., Nabavinia, M., Binth Mohammad, N., Ryan, J., Pourmand, A., Laukaitis, E., Banan Sadeghian, R., Nadhman, A.J.B., 2016. Biomicrofluidics 10 (4), 044111.
Moutaux, E., Charlot, B., Genoux, A., Saudou, F., Cazorla, M., 2018. Lab Chip 18 (22), 3425–3435.
Mueller, B.J., Zhdanov, A.V., Borisov, S.M., Foley, T., Okkelman, I.A., Tsytsarev, V., Tang, Q., Erzurumlu, R.S., Chen, Y., Zhang, H., Toncelli, C., Klimant, I., Papkovsky, D.B., Dmitriev, R.I., 2018. Adv. Funct. Mater. 28 (9).
Muguruma, K., Nishiyama, A., Kawakami, H., Hashimoto, K., Sasai, Y., 2015. Cell Rep. 10 (4), 537–550.
Nadzirah, S., Gopinath, S.C., Parmin, N., Hamzah, A.A., Mohamed, M.A., Chang, E.Y., Dee, C.F., 2022. Crit. Rev. Anal. Chem. 52 (3), 637–648.
Nag, S., 2003. The blood-brain barrier 3–36.
Nangare, S., Patil, P., 2022. Int. J. Biol. Macromol. 214, 568–582.
Nasr, B., Chatterton, R., Yong, J.H.M., Jamshidi, P., D'Abaco, G.M., Bjorksten, A.R., Kavehei, O., Chana, G., Dottori, M., Skafidas, E.J.B., 2018. Biosensors 8 (1), 14.
Ndyabawe, K., Cipriano, M., Zhao, W., Haidekker, M., Yao, K., Mao, L., Kisaalita, W.S., 2020. ACS Biomater. Sci. Eng. 7 (1), 350–359.

Neniskyte, U., Vilalta, A., Brown, G.C., 2014. FEBS Lett. 588 (17), 2952–2956.
Niaraki, A., Abbasi Shirsavar, M., Aykar, S.S., Taghavimehr, M., Montazami, R., Hashemi, N.N., 2022. Biosens. Bioelectron. 210, 114284.
Nielsen, J.B., Hanson, R.L., Almughamsi, H.M., Pang, C., Fish, T.R., Woolley, A.T., 2019. Anal. Chem. 92 (1), 150–168.
Nieus, T., D'Andrea, V., Amin, H., Di Marco, S., Safaai, H., Maccione, A., Berdondini, L., Panzeri, S., 2018. Sci. Rep. 8 (1), 5578.
Obien, M.E.J., Deligkaris, K., Bullmann, T., Bakkum, D.J., Frey, U., 2015. Front. Neurosci. 8, 423.
Oddo, A., Peng, B., Tong, Z., Wei, Y., Tong, W.Y., Thissen, H., Voelcker, N.H., 2019. Trends Biotechnol. 37 (12), 1295–1314.
Odijk, M., van der Meer, A.D., Levner, D., Kim, H.J., van der Helm, M.W., Segerink, L.I., Frimat, J.P., Hamilton, G.A., Ingber, D.E., van den Berg, A., 2015. Lab Chip 15 (3), 745–752.
Oh, J., Yoo, G., Chang, Y.W., Kim, H.J., Jose, J., Kim, E., Pyun, J.-C., Yoo, K.-H., 2013. Biosens. Bioelectron. 50, 345–350.
Oliver, C.R., Altemus, M.A., Westerhof, T.M., Cheriyan, H., Cheng, X., Dziubinski, M., Wu, Z., Yates, J., Morikawa, A., Heth, J., 2019. Lab Chip 19 (7), 1162–1173.
Ostuni, E., Kane, R., Chen, C.S., Ingber, D.E., Whitesides, G.M., 2000. Langmuir 16 (20), 7811–7819.
Özsoylu, D., Wagner, T., Schöning, M.J., 2022. Curr. Top. Med. Chem. 22 (9), 713–733.
Park, J., Lee, B.K., Jeong, G.S., Hyun, J.K., Lee, C.J., Lee, S.-H., 2015. Lab Chip 15 (1), 141–150.
Park, S.E., Georgescu, A., Huh, D., 2019a. Science 364 (6444), 960–965.
Park, T.-E., Mustafaoglu, N., Herland, A., Hasselkus, R., Mannix, R., FitzGerald, E.A., Prantil-Baun, R., Watters, A., Henry, O., Benz, M., 2019b. Nat. Commun. 10 (1), 1–12.
Partyka, P.P., Godsey, G.A., Galie, J.R., Kosciuk, M.C., Acharya, N.K., Nagele, R.G., Galie, P.A., 2017. Biomaterials, 115, pp. 30–39.
Paşca, A.M., Sloan, S.A., Clarke, L.E., Tian, Y., Makinson, C.D., Huber, N., Kim, C.H., Park, J.-Y., O'Rourke, N.A., Nguyen, K.D., 2015. Nat. Methods 12 (7), 671–678.
Pediaditakis, I., Kodella, K.R., Manatakis, D.V., Le, C.Y., Hinojosa, C.D., Tien-Street, W., Manolakos, E.S., Vekrellis, K., Hamilton, G.A., Ewart, L., 2021a. Nat. Commun. 12 (1), 1–17.
Pediaditakis, I., Kodella, K.R., Manatakis, D.V., Le, C.Y., Hinojosa, C.D., Tien-Street, W., Manolakos, E.S., Vekrellis, K., Hamilton, G.A., Ewart, L., Rubin, L.L., Karalis, K., 2021b. Nat. Commun. 12 (1), 5907.
Pelkonen, A., Mzezewa, R., Sukki, L., Ryynanen, T., Kreutzer, J., Hyvarinen, T., Vinogradov, A., Aarnos, L., Lekkala, J., Kallio, P., Narkilahti, S., 2020. Biosens. Bioelectron. 168, 112553.
Perestrelo, A.R., Águas, A.C., Rainer, A., Forte, G., 2015. Sensors 15 (12), 31142–31170.
Petrovszki, D., Walter, F., Vigh, J., Kocsis, A., Valkai, S., Deli, M., Dér, A., 2022. Biomedicines 10 (1), 188.
Peyrin, J.-M., Deleglise, B., Saias, L., Vignes, M., Gougis, P., Magnifico, S., Betuing, S., Pietri, M., Caboche, J., Vanhoutte, P., 2011. Lab Chip 11 (21), 3663–3673.
Phan, D.T.T., Bender, R.H.F., Andrejecsk, J.W., Sobrino, A., Hachey, S.J., George, S.C., Hughes, C.C.W., 2017. Exp. Biol. Med. 242 (17), 1669–1678.
Picciolini, S., Gualerzi, A., Vanna, R., Sguassero, A., Gramatica, F., Bedoni, M., Masserini, M., Morasso, C., 2018. Anal. Chem. 90 (15), 8873–8880.
Piliarik, M., Vaisocherová, H., Homola, J., 2009. Biosensors and Biodetection 65–88.
Pitsalidis, C., Ferro, M., Iandolo, D., Tzounis, L., Inal, S., Owens, R., 2018. Sci. Adv. 4 (10), eaat4253.
Prabhakarpandian, B., Shen, M.-C., Nichols, J.B., Mills, I.R., Sidoryk-Wegrzynowicz, M., Aschner, M., Pant, K., 2013. Lab Chip 13 (6), 1093–1101.
Prodanov, D., Delbeke, J., 2016. Front. Neurosci. 10, 11.
Pulido, R.S., Munji, R.N., Chan, T.C., Quirk, C.R., Weiner, G.A., Weger, B.D., Rossi, M.J., Elmsaouri, S., Malfavon, M., Deng, A., Profaci, C.P., Blanchette, M., Qian, T., Foreman, K.L., Shusta, E.V., Gorman, M.R., Gachon, F., Leutgeb, S., Daneman, R., 2020. Genes. Neuron 108 (5), 937–952 e937.
Puryear Iii, J.R., Yoon, J.-K., Kim, Y., 2020. Micromachines 11 (8), 730.
Qian, X., Nguyen, H.N., Song, M.M., Hadiono, C., Ogden, S.C., Hammack, C., Yao, B., Hamersky, G.R., Jacob, F., Zhong, C., 2016. Cell 165 (5), 1238–1254.
Qian, X., Jacob, F., Song, M.M., Nguyen, H.N., Song, H., Ming, G.-l., 2018. Nat. Protoc. 13 (3), 565–580.
Qin, J., Wang, W., Gao, L., Yao, S., 2022. Chem *13* (10), 2857–2876.
Ravi, M., Paramesh, V., Kaviya, S.R., Anuradha, E., Solomon, F.D.P., 2015. J. Cell. Physiol. 230 (1), 16–26.
Rezaei, B., Irannejad, N., 2019. Electrochemical Biosensors. Elsevier, pp. 11–43.
Ricco, A.J., Martin, S.J., 1991. Thin Solid Films 206 (1–2), 94–101.
Rickard, J.J., Di-Pietro, V., Smith, D.J., Davies, D.J., Belli, A., Oppenheimer, P.G., 2020. Nature Biomedical Engineering 4 (6), 610–623.
Roberts, S., Seeger, M., Jiang, Y., Mishra, A., Sigmund, F., Stelzl, A., Lauri, A., Symvoulidis, P., Rolbieski, H., Preller, M., Dean-Ben, X.L., Razansky, D., Orschmann, T., Desbordes, S.C., Vetschera, P., Bach, T., Ntziachristos, V., Westmeyer, G.G., 2018. J. Am. Chem. Soc. 140 (8), 2718–2721.
Rodrigues, R.O., Sousa, P.C., Gaspar, J., Bañobre-López, M., Lima, R., Minas, G., 2020. Small 16 (51), 2003517.
Ronchi, S., Buccino, A.P., Prack, G., Kumar, S.S., Schroter, M., Fiscella, M., Hierlemann, A., 2021. Adv Biol (Weinh) 5 (3), e2000223.
Rothbauer, M., Ertl, P., 2020. Microfluidics in Biotechnology 343–354.
Ryynänen, T., Pelkonen, A., Grigoras, K., Ylivaara, O.M.E., Hyvärinen, T., Ahopelto, J., Prunnila, M., Narkilahti, S., Lekkala, J., 2019. Front. Neurosci. 13.
Salahandish, R., Hassani, M., Zare, A., Haghayegh, F., Sanati-Nezhad, A., 2022. Lab Chip 22 (8), 1542–1555.
Samarasinghe, R.A., Miranda, O.A., Buth, J.E., Mitchell, S., Ferando, I., Watanabe, M., Allison, T.F., Kurdian, A., Fotion, N.N., Gandal, M.J., Golshani, P., Plath, K., Lowry, W.E., Parent, J.M., Mody, I., Novitch, B.G., 2021. Nat. Neurosci. 24 (10), 1488–1500.
Samper, I., Gowers, S., Rogers, M., Murray, D., Jewell, S., Pahl, C., Strong, A., Boutelle, M., 2019. Lab Chip 19 (11), 2038–2048.
Sellgren, K.L., Hawkins, B.T., Grego, S., 2015. Biomicrofluidics 9 (6), 061102.
Senel, M., Dervisevic, E., Alhassen, S., Dervisevic, M., Alachkar, A., Cadarso, V.J., Voelcker, N.H., 2020. Anal. Chem. 92 (18), 12347–12355.
Seyhan, A.A., 2019. Translational Medicine Communications 4 (1), 18.
Seymour, J.P., Wu, F., Wise, K.D., Yoon, E., 2017. Microsyst Nanoeng 3, 16066.
Sharabi, Y., Vatine, G.D., Ashkenazi, A., 2021. Lancet Neurol. 20 (10), 868–876.
Shen, X., Wu, J., Wang, Z., Chen, T., 2019. Electrophoresis 40 (22), 2996–3004.
Shi, M., Majumdar, D., Gao, Y., Brewer, B.M., Goodwin, C.R., McLean, J.A., Li, D., Webb, D.J., 2013. Lab Chip 13 (15), 3008–3021.
Shi, Y., Sun, L., Wang, M., Liu, J., Zhong, S., Li, R., Li, P., Guo, L., Fang, A., Chen, R., 2020. PLoS Biol. 18 (5), e3000705.
Shin, H., Jeong, S., Lee, J.-H., Sun, W., Choi, N., Cho, I.J., 2021. Nat. Commun. 12 (1), 492.
Shirure, V.S., George, S.C., 2017. Lab Chip 17 (4), 681–690.
Song, C., Deng, P., Que, L., 2018. Nanomed. Nanotechnol. Biol. Med. 14 (6), 1845–1852.
Song, C., Que, S., Heimer, L., Que, L., 2020. Micromachines 11 (7), 629.
Soscia, D.A., Lam, D., Tooker, A.C., Enright, H.A., Triplett, M., Karande, P., Peters, S.K. G., Sales, A.P., Wheeler, E.K., Fischer, N.O., 2020. Lab Chip 20 (5), 901–911.
Spijkers, X.M., Pasteuning-Vuhman, S., Dorleijn, J.C., Vulto, P., Wevers, N.R., Pasterkamp, R.J., 2021. Sci. Rep. 11 (1), 1–15.
Strakosas, X., Bongo, M., Owens, R.M., 2015. J. Appl. Polym. Sci. 132 (15).
Subia, B., Dahiya, U.R., Mishra, S., Ayache, J., Casquillas, G.V., Caballero, D., Reis, R.L., Kundu, S.C., 2021. J. Contr. Release 331, 103–120.
Subramanian, S., Wu, H.Y., Constant, T., Xavier, J., Vollmer, F., 2018. Adv. Mater. 30 (51), 1801246.
Sullivan, K.M., Ko, E., Kim, E.M., Ballance, W.C., Ito, J.D., Chalifoux, M., Kim, Y.J., Bashir, R., Kong, H.J., 2022. Tissue Eng. B Rev. 28 (6), 1209–1222.
Syama, S., Mohanan, P.V., 2021. Trends Food Sci. Technol. 110, 711–728.
Takata, F., Nakagawa, S., Matsumoto, J., Dohgu, S., 2021. Front. Cell. Neurosci. 15, 661838.
Taly, V., Kelly, B.T., Griffiths, A.D., 2007. Chembiochem 8 (3), 263–272.
Tanner, K., Gottesman, M.M., 2015. Sci. Transl. Med. 7 (283), 283ps289-283ps289.
Taylor, A.M., Blurton-Jones, M., Rhee, S.W., Cribbs, D.H., Cotman, C.W., Jeon, N.L., 2005. Nat. Methods 2 (8), 599–605.
Teleanu, R.I., Preda, M.D., Niculescu, A.-G., Vladăcenco, O., Radu, C.I., Grumezescu, A. M., Teleanu, D.M., 2022. Pharmaceutics 14 (5), 987.
Terrell-Hall, T.B., Ammer, A.G., Griffith, J.I.G., Lockman, P.R., 2017. Fluids Barriers CNS 14 (1), 1–10.
Tong, Z., Segura-Feliu, M., Seira, O., Homs-Corbera, A., Del Río, J.A., Samitier, J., 2015. RSC Adv. 5 (90), 73457–73466.
Tong, Z., Kwak, E., Aguiar, A., Peng, B., Pouton, C.W., Voelcker, N.H., Haynes, J.M., 2021. Lab Chip 21 (20), 4016–4030.
Touhami, A., 2014. Nanomedicine 15, 374–403.
Ugolini, G.S., Occhetta, P., Saccani, A., Re, F., Krol, S., Rasponi, M., Redaelli, A., 2018. J. Micromech. Microeng. 28 (4).
Unger, C., Kramer, N., Walzl, A., Scherzer, M., Hengstschlaeger, M., Dolznig, H., 2014. Adv. Drug Deliv. Rev. 79, 50–67.
van de Wijdeven, R., Ramstad, O.H., Valderhaug, V.D., Kollensperger, P., Sandvig, A., Sandvig, I., Halaas, O., 2019. Biosens. Bioelectron. 140, 111329.
Vatine, G.D., Barrile, R., Workman, M.J., Sances, S., Barriga, B.K., Rahnama, M., Barthakur, S., Kasendra, M., Lucchesi, C., Kerns, J., 2019. Cell Stem Cell 24 (6), 995–1005 e1006.
Vieira de Sá, R., Cañizares Luna, M., Pasterkamp, R.J., 2021. Tissue Eng. C Methods 27 (3), 213–224.
Vinci, M., Gowan, S., Boxall, F., Patterson, L., Zimmermann, M., Lomas, C., Mendiola, M., Hardisson, D., Eccles, S.A., 2012. BMC Biol. 10 (1), 1–21.
Virlogeux, A., Moutaux, E., Christaller, W., Genoux, A., Bruyere, J., Fino, E., Charlot, B., Cazorla, M., Saudou, F., 2018. Cell Rep. 22 (1), 110–122.
Virlogeux, A., Scaramuzzino, C., Lenoir, S., Carpentier, R., Louessard, M., Genoux, A., Lino, P., Hinckelmann, M.-V., Perrier, A.L., Humbert, S., 2021. Sci. Adv. 7 (14), eabb0799.
Viswam, V., Obien, M.E.J., Franke, F., Frey, U., Hierlemann, A., 2019. Front. Neurosci. 13, 385.
Vitrac, A., Cloëz-Tayarani, I., 2018. Stem Cell Res. Ther. 9 (1), 1–7.
Wang, D.S., Fan, S.K., 2016. Sensors 16 (8), 1175.
Wang, X., Hou, Y., Ai, X., Sun, J., Xu, B., Meng, X., Zhang, Y., Zhang, S., 2020. Biomed. Pharmacother. 132, 110822.
Wang, P., Xu, G., Qin, L., Xu, Y., Li, Y., Li, R., 2005. Sensor. Actuator. B Chem. 108 (1–2), 576–584.
Wang, Y.I., Abaci, H.E., Shuler, M.L., 2017. Biotechnol. Bioeng. 114 (1), 184–194.
Weisenburger, S., Vaziri, A., 2018. Annu. Rev. Neurosci. 41, 431–452.
Weltin, A., Hammer, S., Noor, F., Kaminski, Y., Kieninger, J., Urban, G.A., 2017. Biosens. Bioelectron. 87, 941–948.
Werner, J., Belz, M., Klein, K.-F., Sun, T., Grattan, K., 2021. Measurement 178, 109323.
Whitesides, G.M., 2006. Nature 442 (7101), 368–373.
Wolff, A., Antfolk, M., Brodin, B., Tenje, M., 2015. J Pharm Sci 104 (9), 2727–2746.
Xiang, Y., Tanaka, Y., Patterson, B., Kang, Y.J., Govindaiah, G., Roselaar, N., Cakir, B., Kim, K.Y., Lombroso, A.P., Hwang, S.M., 2017. Cell Stem Cell 21 (3), 383–398.
Xie, Y., Dai, L., Yang, Y., 2022. Biosens. Bioelectron. X 10, 100109.
Xu, Z., Fang, P., Xu, B., Lu, Y., Xiong, J., Gao, F., Wang, X., Fan, J., Shi, P., 2018. Nat. Commun. 9 (1), 1–11.
Yaldiz, B., Saglam-Metiner, P., Yesil-Celiktas, O., 2022. Expet Rev. Mol. Med. 23.

Yang, I.H., Gary, D., Malone, M., Dria, S., Houdayer, T., Belegu, V., McDonald, J.W., Thakor, N., 2012. NeuroMolecular Med. 14 (2), 112–118.
Yang, Q., Lian, Q., Xu, F., 2017. Biomicrofluidics 11 (3), 031301.
Yoo, Y., Kim, J., Kim, G., Kim, Y., Kim, H., Lee, S., 2017. Sci. Rep. 7 (1), 1–10.
Yoon, J.K., Kim, J., Shah, Z., Awasthi, A., Mahajan, A., Kim, Y., 2021. Advanced Healthcare Materials 10 (15), 2002285.
Yu, Y., Shamsi, M.H., Krastev, D.L., Dryden, M.D., Leung, Y., Wheeler, A.R., 2016. Lab Chip 16 (3), 543–552.
Yu, Y., de Campos, R.P., Hong, S., Krastev, D.L., Sadanand, S., Leung, Y., Wheeler, A.R., 2019. Microsystems & Nanoengineering 5 (1), 1–13.
Yu, F., Kumar, N.D.O.S., Foo, L.C., Ng, S.H., Hunziker, W., Choudhury, D.J.B., 2020. Bioengineering. Biotechnol. Bioeng. 117 (4), 1127–1136.
Zare, E.N., Agarwal, T., Zarepour, A., Pinelli, F., Zarrabi, A., Rossi, F., Ashrafizadeh, M., Maleki, A., Shahbazi, M.A., Maiti, T.K., 2021. Appl. Mater. Today 24, 101117.
Zhang, F., Qu, K.Y., Zhou, B., Luo, Y., Zhu, Z., Pan, D.J., Cui, C., Zhu, Y., Chen, M.L., Huang, N.P., 2021. Biosens. Bioelectron. 179, 113080.
Zhao, S., Yang, M., Zhou, W., Zhang, B., Cheng, Z., Huang, J., Zhang, M., Wang, Z., Wang, R., Chen, Z., 2017. Proc. Natl. Acad. Sci. USA 114 (35), E7245–E7254.
Zhao, F., Zhong, L., Luo, Y., 2021. CNS Neurosci. Ther. 27 (1), 26–35.
Zhao, Y., Liu, Y., Xu, Y., Li, K., Zhou, L., Qiao, H., Xu, Q., Zhao, J., 2022. Cell. Mol. Neurobiol. 1–14.
Zheng, F., Fu, F., Cheng, Y., Wang, C., Zhao, Y., Gu, Z., 2016. Small 12 (17), 2253–2282.
Zhou, W.M., Yan, Y.Y., Guo, Q.R., Ji, H., Wang, H., Xu, T.T., Makabel, B., Pilarsky, C., He, G., Yu, X.Y., Zhang, J.Y., 2021. J. Nanobiotechnol. 19 (1), 312.
Zhu, Y., Mandal, K., Hernandez, A.L., Kawakita, S., Huang, W., Bandaru, P., Ahadian, S., Kim, H.J., Jucaud, V., Dokmeci, M.R., 2021. Current Opinion in Biomedical Engineering 19, 100309.